Universitat de les Illes Balears

MASTER'S THESIS

Elastic and Anelastic Magnetomechanical Phenomena Close to the Premartensitic Transition in Ni-Mn-Ga

Jaime Rosselló Coll

Master's Degree in Advanced Physics and Applied Mathematics

Materials Science

Centre for Postgraduate Studies

Academic Year 2021-22

Elastic and Anelastic Magnetomechanical Phenomena Close to the Premartensitic Transition in Ni-Mn-Ga

Jaime Rosselló Coll

Master's Thesis

Centre for Postgraduate Studies

University of the Balearic Islands

Academic Year 2021-22

Key words:

SMA, FMSMA, Magnetic Domains, Premartenstic Transition, Eddy Currents.

Thesis Supervisor's Name: Jaume Pons

Tutor's Name: Sergey Kustov

Content:

Abstract 5

1. Introduction 6

1.1. Martensitic transformation and precursor phenomena 6

1.2. Ni-Mn-Ga system alloys 8

1.3. Precursor Phenomena in Ni2MnGa 9

1.3.1. A brief summary of previous studies 10

1.3.2. Additional softening due to magnetoelastic coupling 12

1.3.3. Softening due to macroscopic magnetization. Domain wall contribution 13

1.4. Magnetomechanical damping: a summary of Microeddy and Macroeddy - current relaxation strength and frequency 17

1.4.1. Macroeddy Current Strength and Frequencies 18

1.4.2. Microeddy Current Strength and Frequencies 21

2. Materials and Experimental Technique 23

2.1. Sample preparation 23

2.2. Experimental procedure 26

3. Results: Analysis 31

3.1. Temperature dependence of the internal friction and Young´s modulus 31

3.1.1. Demagnetized State 31

3.1.2. Moderate Fields 34

3.2. Strain amplitude dependence of the internal friction and resonant frequency 34

3.3. Applied field dependences of the internal friction and Young´s modulus 43

4. Interpretation of results *46*

4.1. Frequency and field dependence of micro- and macroeddy internal friction and modulus defect *46*

4.2. Parameters affecting Microeddy and Macroeddy current relaxations during premartensitic transformation in Ni2MnGa. *49*

4.2.1. Eddy current relaxation frequencies during PMT, Eqs. 4.6 and 4.7 ..... *50*

4.2.2. Eddy current relaxation strengths during PMT *50*

4.3. Interpretation of the anelastic and "elastic" phenomena during PMT as due to the eddy current relaxations *53*

5. Conclusions *55*

6. References *56*

Annex: Copy of the published article, Kustov, S.; Rosselló, J.; Corró, M. L.; Kaminskii, V.; Sapozhnikov, K.; Saren, A.; Sozinov A. and Ullakko, K.; Magnetic Domain Walls and Macroscopic Magnetization-Related Elastic and Anelastic Effects during Premartensitic Transition in Ni_2MnGa, Materials, 12, (2019), p376.

Abstract:

The temperature and field dependences of internal friction (IF) and Young's modulus (YM) are studied using longitudinal resonant oscillations (90 kHz) technique in stoichiometric ferromagnetic Ni_2MnGa single crystal along the [100] direction, close to the premartensitic transformation temperature, T_{PM}, in the demagnetized state and under moderate fields. It is shown that: the apparent Young's modulus softens close to T_{PM} under moderate fields, instead of the hardening outside this range. This effect and other previously reported as the splitting IF peak and YM minimum damping during premartensitic transition are interpreted in terms of superposition of classical magnetic domain wall -related Microeddy and Macroeddy current relaxations, which have not been considered so far as the origin of premartensitic anelastic effects in Ni_2MnGa.

1. Introduction

1.1. Martensitic transformation and precursor phenomena

Martensitic transformation (MT) is a typical solid-state displacive and diffusionless (no atomic diffusion) first-order phase transition that breaks crystal symmetry by development of spontaneous anisotropic lattice strain upon cooling. Lattice strain dominates the morphology of the low-temperature low-symmetry phase (called martensite) and the kinetics of the transformation. Since steels in the martensitic state proved to have an increased hardness, this solid-solid phase transition received a large amount of attention regarding its advantages in the construction sector.

Apart from steels, this kind of transformation has been observed over the years in a wide range of different materials, such as pure metals and non-ferrous alloys, inorganic compounds, polymers, and surprisingly even in some bacteria [1]. After the discovery of the MT in compounds other than steels, some of the most important useful effects that exhibit this transformation were revealed. These properties are the Thermoelasticity, the Super Elasticity (SE) and the Shape Memory Effect (SME). The last two properties are closely linked to the MT, but not all materials that exhibit a MT will present SE and SME [2-4]. Those materials that possess SE and SME are conventionally referred to as Shape Memory Alloys (SMA).

Two different crystallographic phases take part in a MT, which have different lattice symmetries: the high temperature phase (austenite) possesses the higher symmetry. In shape memory alloys, usually, it has cubic symmetry. On the other hand, the low temperature phase (martensite) has a lower symmetry and the crystallographic phase can be tetragonal, trigonal, orthorhombic, monoclinic or triclinic. Then, an orientation relationship exists between the high symmetry and low symmetry phases. When an element of the high symmetry phase transforms into the low symmetry phase, it can adopt different orientations which are compatible with the one of the parent phase: in extension, there is a certain number of atomic configurations which are energetically equivalent, but have several different crystallographic orientations. Each one of these possible orientations in martensite is called a martensitic variant or elastic domain [2]. Martensite in general and shape memory alloys can be non-magnetic or ferromagnetic (magnetically ordered). The latter case corresponds to the ordering of both lattice strain and magnetic moments. The ferromagnetic martensites, therefore, possess two

ferroic properties and can be considered as multiferroic materials. Coupling between these two ferroic properties becomes of a prime importance in application of ferromagnetic shape memory alloys. The most attractive and promising is magnetic actuation, when the applied magnetic field results in large so-called magnetostrains. The magnetostrain is due to the rearrangement of the martensitic variant structure by applied field.

Because of the nature of the martensitic transformation, involving lattice strain, martensite is subjected to high stresses that can result in plastic deformation. However, the particular configuration of the martensitic variants (needles/plates) and their mutual arrangement contribute to decrease the deformation energy. A first order structural transition requires the stages of nucleation of a new phase and of the growth of the nuclei. To reduce these stresses during nucleation, the new phase grows from different nuclei with different crystallographic orientations, forming finally different variants of martensite that accommodate the shape and volume change during the MT. Such polyvariant structure eliminates also the possible macroscopic deformation of the sample. However, if a single crystal of austenite transforms into a single variant of martensite, the self-accommodation of the structural variants (twin-related) produced during the martensitic transformation, results in the macroscopic strain of the sample [2].
Another important characteristic of martensitic phases is the internal substructure of variants. The variants may contain twins or stacking faults that allow the habit plane that separates martensite and austenite during MT to be invariant (i.e. its atoms belong to both phases simultaneously).

An interesting feature of martensitic transitions in shape memory alloys is the existence of the precursor phenomena. They reflect that, in a sense, the system prepares for the phase transition before it actually takes place [5]. They are a consequence of weak restoring forces in specific crystallographic directions that announce the possibility of dynamic instability [6].

In particular, when approaching the martensitic transformation temperature from above, the high-temperature phase, which corresponds to a cubic austenitic phase, is expected to exhibit an increasing shear instability. This feature is observed in magnetic and non-magnetic shape-memory alloys [7, 8]. It is generally agreed that in Magnetic Shape Memory Alloys (MSMA), the structural lattice softening near the premartensitic transition can be affected by magnetoelastic coupling [5, 9, 10].

1.2. Ni-Mn-Ga system alloys

Ni-Mn-Ga are archetypal magnetic shape memory alloys with different sequences of magnetic and structural transitions that demonstrate unique physical properties. This intermetallic compound exhibits a martensitic transition from a high temperature Heusler structure towards a more close-packed phase. Regarding their properties, the largest magnetostrain effects have been observed in Ni-Mn-Ga-based Heusler alloys, where up to 6% and 12% strains have been induced by a magnetic field [11].

A number of thermal and stress-induced martensitic transformations has been observed in Ni_2MnGa alloys, and numerous experiments concluded that both transition temperatures and crystallographic structures are quite sensitive to alloy composition. For example, $Ni_{2.18}Mn_{0.82}Ga$ raises MT to 340K whereas the MT of $Ni_{2.16}Mn_{0.84}Ga$ reaches 532K [13, 15, 16].

Depending on the composition (more specifically, on the electron/atom ratio) and values of the MT temperatures these alloys have been conventionally classified into three groups [12].

1 - Alloys with $T_M < room\ temp\ and\ Tc \approx 370K$

2 - Alloys with $T_M \approx 370K, but\ below\ Tc$

3 - Alloys with $T_M > Tc$

In the near stoichiometric Ni_2MnGa, which is ferromagnetic below $T_C \approx 380K$, two thermally induced transformations have been observed. A premartensitic phase transformation from the high temperature cubic Heusler structure to a non-uniform at the nanoscale structure with overall cubic symmetry occurs around $T_{PM} \approx 260K$, followed by the martensitic transformation to a 3M modulated tetragonal structure below $T_M \approx 220K$. The low temperature martensitic phase has high magnetocrystalline anisotropy, making it useful for actuator applications [13, 14].

1.3. Precursor Phenomena in Ni_2MnGa

The structural transitions in near stoichiometric Ni_2MnGa have been widely studied over the last 3 decades, being subject of a large number of experimental and theoretical studies. The important parts of these studies are the interpretations of evolution of the individual phases with temperature [9].

In particular, the precursor phenomena has been observed by different experimental techniques such as X-ray, electron-neutron scattering, ultrasonic measurements, transmission-electron microscopy and differential scanning calorimetry (Figure 1.1) among others [17].

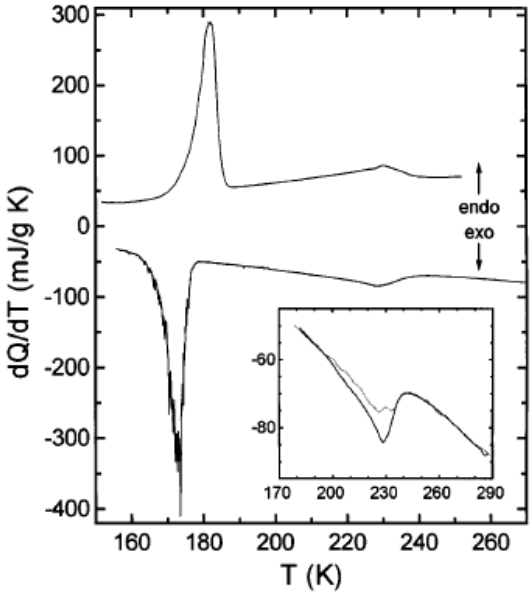

Figure 1.1: Differential scanning calorimetry on Ni_2MnGa sample. The small peak shows a premartensitic transition at around 230 K. The inset shows the premartensitic peak with the measured base line for evaluation of the latent heat [5].

The origin of the premartensitic transition, the premartensitic structure and the premartensitic effects persist as a research topic. In the austenitic $L2_1$ Heusler structure of Ni_2MnGa, an important role of magnetoelastic coupling and lattice softening has traditionally been postulated: softening effect is assigned to a phonon condensation with q=0.33 wave vector associated with the TA_2 acoustic branch, and softening of the shear elastic constant C' [18].

TA_2 phonon anomalies have been evidenced by Inelastic Neutron-Scattering studies [19]. Moreover, the existence of this soft phonon mode gave rise to diffuse X-Ray and Electron Scattering experiments at temperatures above martensitic transition. The results evidenced that when cooling down the sample, this effect became more pronounced, yet the softening was incomplete and below a given temperature the frequency of the modes started to increase again [18, 20].

Thereafter, Transmission Electron Microscopy (TEM) experiments provided information about the formation of modulated structures at the nano-scale level. When we reach temperatures of T_{PM} ($T_{PM} > T_M$) a micromodulated structure that precedes the

martensitic phase appears. This micromodulated structure is indicative of some mesoscopic lattice deformation that anticipates the upcoming martensitic transition, and it has been defined as a result of coherent nanodispersive tetragonal perturbations (clusters/domains) embedding in the parent phase at the initial state of the martensitic transition that form regular patterns called tweeds [21, 22, 23].

The premartensitic tweed morphology is a characteristic cross-hatched nanoscale striation which matches neither the parent phase nor the product phase, as it is shown in Figure 1.2 [24]. The tweed structure appears in near stoichiometric Ni_2MnGa, when the structural disorder is minimal. Besides the discussion whether the modulation is commensurate [25] or incommensurate [26], following recent model by Seiner et al. [27], the premartensitic phase in Ni_2MnGa is formed by nanoscopic tetragonal blocks distributed randomly in all possible orientations [27]. Figure 1.3 shows schematically the microstructure of premartensitic phase in Ni_2MnGa as suggested by Seiner et al [27]. Such heterogeneous on the nanoscale structure has an average cubic symmetry, in full agreement with the experimental observations.

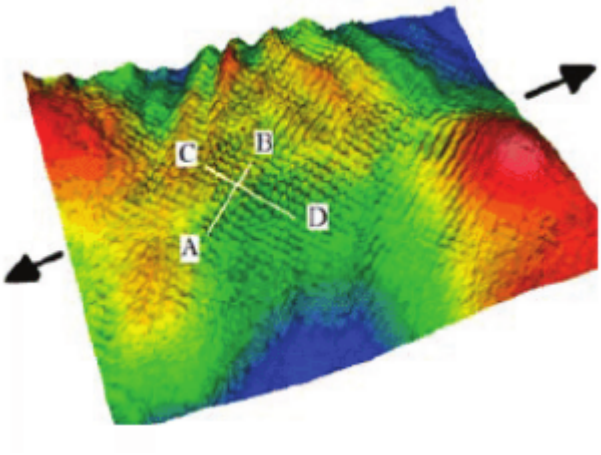

Figure 1.2: Tweed structure on the surface of an aluminium polycrystalline foil. [24]

1.3.1. A brief summary of previous studies

Magnetic, elastic and anelastic properties of a complicated nanoheterogeneous structure shown in Fig. 1.3 are difficult to predict and explain. Several Pulse-echo ultrasonic studies were used to determine the elastic constants along the premartensitic transition [5, 17, 27, 28]. As an example, Worgull et al. [28] measured the elastic constants at 265K using this technique. Comparing the results with other ones obtained by electromagnetic generation technique (EMG) [21], they have shown that the error obtained in C' values was more than 1600%, which illustrated the structural instability of the phase transition.

Later on, with the same technique, Stipcich et al. [29] measured the elastic constants of two Ni_2MnGa samples close to the stoichiometric composition ($Ni_{52.0}Mn_{23.0}Ga_{25}$ and $Ni_{50.5}Mn_{29.5}Ga_{20.0}$) along the [001] direction. They concluded that the strong attenuation of the shear waves associated with this direction makes the value of C' difficult to characterize accurately, and also admitted that the values were affected by a considerable error.

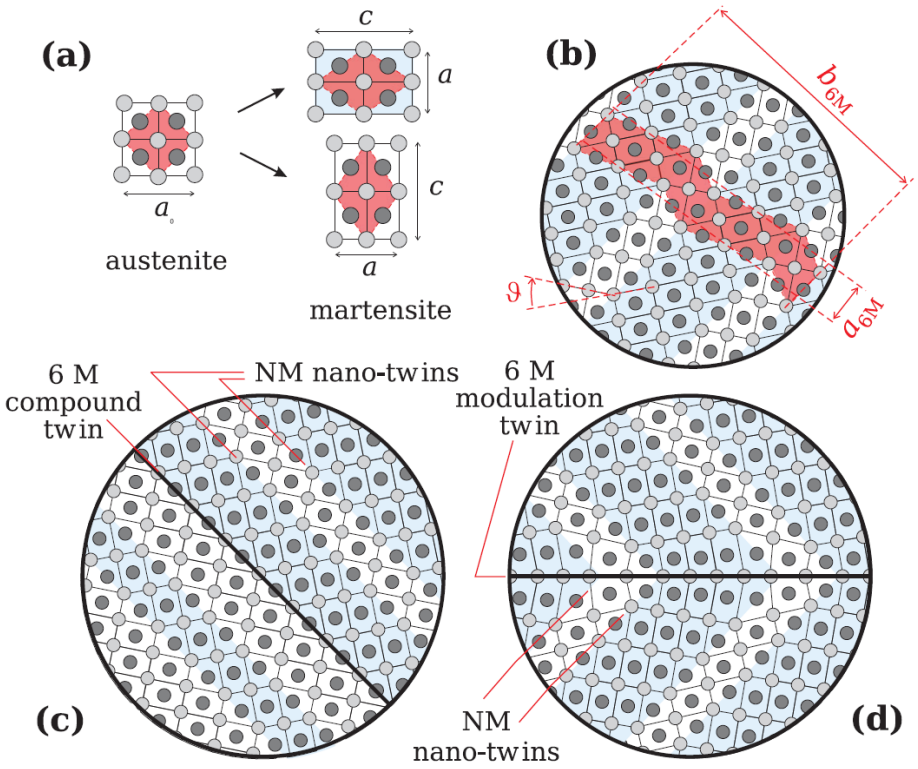

Figure 1.3: Schematic representation of a two-dimensional model for premartensitic tweed in Ni2MnGa (taken from [27]): (a): cubic unit cell of austenite that transforms into two possible orientations of tetragonal martensite; (b) construction of 6M modulated structure marked in red from tetragonal units. (c), (d) two types of twins in 6M structure which result in an average cubic symmetry of the lattice..

In other cases the elastic constants were determined by resonant ultrasound spectroscopy (RUS) [30, 31]. This method, more sensitive to C' and insensitive to C_{11} and C_{44} [32] and used along the [100] direction, permitted to obtain the absolute value of Young Modulus in the cubic Ni_2MnGa (since $E_{100} \approx 3C'$). A general tendency in initial works was to neglect the potential role of magnetic domains in the premartensitic effects in general and in elastic and anelastic effects in particular.

1.3.2. The additional softening due to magnetoelastic coupling

One of the first attempts to explain the premartensitic effects in Ni_2MnGa was developed by Planes et al [5], who constructed a Landau-type model for the first order PMT using three parameters:

The primary order parameter is the amplitude η of the TA_2 [110] phonon, and secondary parameters are ε (a (110) [1-10] homogenous shear suitable to describe a cubic to tetragonal change of symmetry) and M, the magnetization of the sample. In terms of these parameters the free energy can be described as:

$$\mathcal{F}(\eta, \varepsilon, M) = F_{str}(\eta, \varepsilon) + F_{mag}(M) + F_{me}(\eta, \varepsilon, M). \quad (1.1)$$

Equation 1.1 includes a structural component $F_{str}(\eta, \varepsilon)$, a magnetic component $F_{mag}(M)$ and a mixed term that accounts the magnetoelastic coupling $F_{me}(\eta, \varepsilon, M)$. Planes et al. eventually related the change of elastic constants with variations of the macroscopic magnetization. However, the variation of macroscopic magnetization is related essentially with the rearrangement of magnetic domain structure and domain walls during PMT rather than with dynamical lattice properties [3].

The role of the magnetoelastic coupling was studied by some researchers, who in their experiments studied the interpretation of the elastic constants softening due to magnetoelastic interaction using this model [32-34]. However, they related the change of elastic constants under a saturating field (which favours the importance of magnetoelastic coupling over dynamical lattice properties regarding the elastic softening) with variations of the macroscopic magnetization, two phenomenological events that cannot be related to explain the softening of elastic constants.

The effect of the magnetic field was studied by Gonzalez-Comas et al [5,6] who analysed the field dependences of the elastic coefficients at room temperature using pulse-echo method, and the experimental results observed were not changing significantly. On the other hand, Zhao et al [35] observed a minor effect using an ultrasonic continuous-wave method, which operates at a frequency of 100 kHz, and found a strong effect of field in a $Ni_{49.0}Mn_{23.5}Ga_{27.5}$ sample along [001] crystallographic direction. These results demonstrate the magnetic signature in the precursor phenomena, which leads to increase the shear stiffness of the lattice and the decrease of the damping coefficient,

and supported the idea of a magnon-phonon coupling and thus, the first order martensitic transition described in the Landau-model. However, the published results were incomplete and rather inconclusive, and evidenced the need for a study that combined the effect of magnetic field and temperature [9].

1.3.3. Softening due to macroscopic magnetization. The domain wall contribution

Unexpectedly, until recent time, the interpretations of acoustic experiments disregarded such important contributions to the anelastic and apparent elastic effects as ferromagnetic domain walls (DW).

Planes et al. [5] presented ultrasonic measurements under an applied field of C' C_{11} and C_{44}. Despite they have observed a minimum of C´ versus field, typical for the macroeddy current relaxation, the minimum was attributed to an experimental error, drawing a line for the expected tendency according to the model presented ($C'=C_{11} + C_{44} - C_L$).

Details on the experiment can be seen in Figure 1.4, where the described solid line proposed by Planes et al. differs from the experimental results obtained (red line).

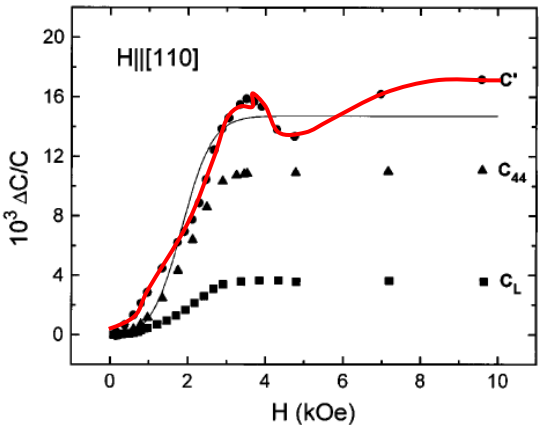

Figure 1.4: Relative change of the elastic constants (solid symbols) as a function of an applied magnetic field H along the [110] direction. The solid line corresponds to C' computed from measured values of C11, C44, and CL.[5]

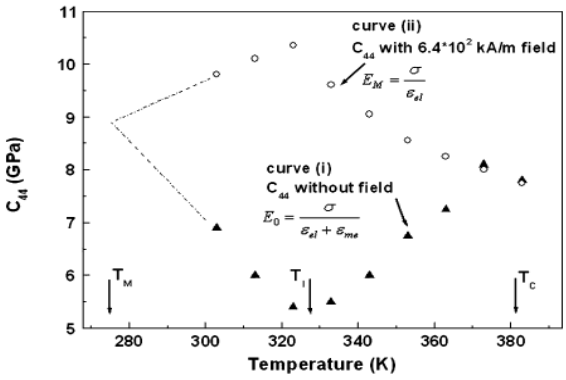

Figure 1.5: Temperature dependence of the elastic constant C44: (i) measured without applying external magnetic field and (ii) high frequency C44 with 6.4x10² kA/m magnetic field applied [36].

Similar conclusions were obtained by Zhao et al. [36] who studied C_{44} and C' elastic constants of a $Ni_{49.0}Mn_{23.5}Ga_{27.5}$ single crystal specimen, using an Ultrasonic Continuous Wave Method (UCWM) operating at the 100-kilohertz range for the determination of C_{44}, and a Cantilever Oscillation Measurement (COM) at a frequency much lower than the ones used in UCWM (it is not specified in the article mentioned). Again, according to Figure 1.5, the results show a strong difference between C_{44} values with and without field, reaching 50%. A dip observed in C_{44} in the demagnetized state at T_{PM}~330K was attributed to a combination of magnetic and martensitic origins. On the other hand, no additional softening of C' was observed at T_{PM} but the authors insist in the magnon-phonon interaction below T_c as the best explanation. However, a discontinuity appears accompanied with an IF peak, that remained unexplained, but again linked to the Landau theory, and hence with magnetoelastic coupling.

Later on, Seiner et al. [9] performed studies on the elastic constants in the demagnetized state and under a magnetic field up to saturation in temperature range of 295-400K, using two different acoustic methods: they studied the field dependencies of C_{11} and C_{44}, using the pulse-echo method (PEM) operating at approx. 50MHz, and the conventional RUS (which was operated at a frequency range of 20-200KHz) to determine the coefficient C'.

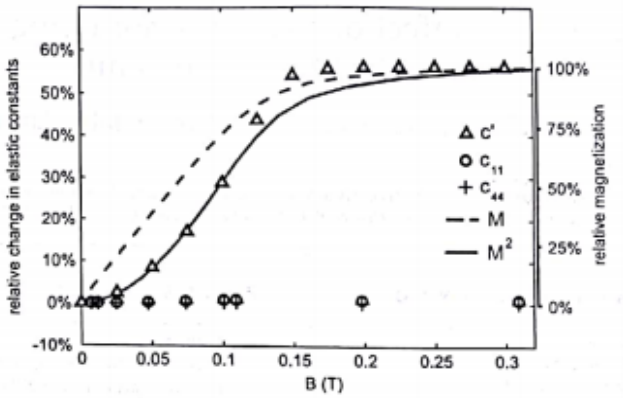

Figure 1.6: Field dependencies of the coefficients C', C_{11} and C_{44} compared to the magnetization curve (M), and the square of magnetization (M^2) [9]

Figure 1.6 shows the field dependences of the elastic components C', C_{44} and C_{11} compared to the magnetization M and the square magnetization M^2. As it can be seen, the difference between C' in zero field and in the saturated state (0.4T) is more than 50%, while the difference in C_{44} and C_{11} is about 0.5% and 1% respectively. Similar minor variation can be observed for the

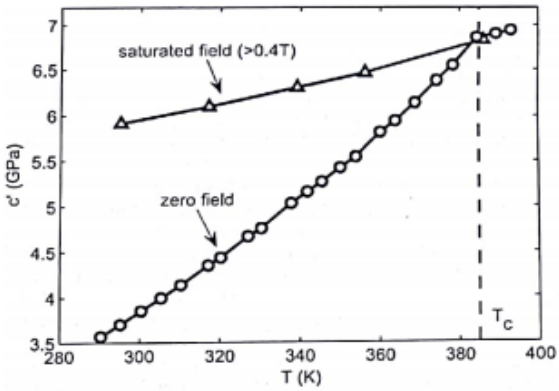

Figure 1.7: Comparison of the C' (T) curves in zero field and in the saturation field. T_C denotes the Curie point. [9]

temperature dependencies of the elastic constants C_{44} and C_L in figure 1.4. However, the data in Fig. 1.4 by Planes et al [5] shows also a very small variation of C´ under field, in dramatic contrast with the data by Seiner. In addition, the data by Zhao et al [36], showing an intense variation of C44 with applied field, Fig. 1.5, strongly contradict the results of both Seiner and Planes.

Finally Figure 1.7 shows that C'decreases monotonously from high temperatures in both demagnetized state and saturated state, but the softening under zero-field is much larger.

C´ in the demagnetized state decreases up to 50% (from 7 GPa at 400K to 3.6 GPa at 290K) with a well-pronounced change of slope at the Curie temperature.

The results reported previously are thus extremely controversial: the same C_{44} and C´ elastic constants show totally different effect of applied field when measured by using RUS or UCWM (at around 10^5 Hz) and PEM (above 10^7 Hz). Due to the effectiveness of the PEM in C_{11} and C_{44}, and the dramatic change provoked in C' using RUS, which is, as the author says, an "unacceptable error", as it can be seen in Figure 1.6. However, they linked the error again with the magnetoelastic effects and the strong anisotropy of Ni-Mn-Ga. The possibility of frequency dispersion in the kHz range was commonly disregarded, assuming that the elastic softening was related with lattice dynamics with much higher characteristic frequencies.

As mentioned in Section 2.1, despite the abundant amount of studies performed with different analysis, the problem seems to match diverse results obtained by this different methods and techniques. Not only the value of C' is affected by considerable error, but also C_{44}, not directly involved in the softening mechanism inherent in martensitic transformations. The reason is the strong frequency dependence of "elastic" constants, where over the range of 10^5 Hz, the softening is much higher than at approximately 10^7 Hz. Therefore, the interpretation should not involve phonon or lattice related elastic effect (which appears in the high MHz and GHz range), but magnetic domain wall relaxations. This also can be seen in Figure 1.5, where the predicted parabolic dependence on M is used to account for the effect of macroscopic magnetization (which is domain structure related) on C´. It is indicative that domain-wall related effects predict precisely this parabolic dependence [36]. As a result, the existence of a characteristic frequency dispersion of apparent elastic and anelastic properties and the interpretation of data presented by Seiner, Zhao and Planes regarding the dependence of the elastic constants with the magnetic field in the kilohertz frequency range suggested the possibility that the additional softening in the premartensitic transition in Ni_2MnGa is caused by the effect of eddy current relaxations.

In 2017, Kustov et al. [37] introduced a new interpretation of the frequency dependence of the apparent elastic and anelastic behaviour due to eddy current relaxations, clarifying the difference between the effect of the magnetic field on the elastic properties and the phonon contribution below the Curie temperature in Ni_2MnGa. The aim of the present work is to try to extend the concept of magnetic domain wall relaxations to the elastic and anelastic effects during PMT.

1.4. Magnetomechanical damping: a brief introduction of Microeddy and Macroeddy current relaxation strength and frequency.

The behaviour of a vibrating ferromagnet in a magnetic field is in general difficult to predict. The formation of magnetic domains, the pinning of their walls, the sample shape and dimensions, anisotropy, and the interaction of applied stress with the domains prevents a general treatment of this problem [38].

It's interesting to remark the similarity between the effects of stress on domain walls and on dislocations that are responsible for non-elastic deformation. This non-elastic deformation (also called anelastic deformation) lags behind the stress by an angle Ø, and is related with the local motion of some micro-structural units that evolves to a new equilibrium value, giving place to a kinetic process with a characteristic relaxation time to be moved into a new equilibrium state [40]. In both cases, the anelastic effects appear as linear damped motions, related with eddy currents in case of ferromagnets, while the hysteretic effects are related with non-linear mode of motion [38]. The contribution of anelastic strains results, in the case of ferromagnets, in the decrease of apparent moduli.

This large decrease in the apparent moduli of the ferromagnet has been called in literature "ΔE effect" based on the assumption that the observed behaviour might be due to a "softening" of the elastic constants as a consequence of the stress-induced domain movement [41]. This softening, which has a correlation with the magnetomechanical damping (MMD) [42] can be seen in the Young's modulus (YM), which in the demagnetized state is normally lower than at saturation [39, 41]:

$$\left(\frac{\Delta E}{E}\right)_{mag} = \frac{E_u - E}{E}, \tag{1.2}$$

where E is the Young Modulus in the relaxed state when magnetic field equals to zero, or lies between zero and the saturation state, and E_u (unrelaxed state) is the Young modulus at saturation.

Following the concepts by Mason [43, 44], Zener [45], and Smith and Birchak [46], three components of magnetomechanical damping arise from anelastic strain: two linear eddy current relaxations, Microeddy and Macroeddy, and a non-linear hysteretic term. In this work only linear relaxational components [43-45] will be treated.

A stress induced change in the net magnetization of an electrically conductive sample produces eventually a transient flow of induced eddy currents which leads to relaxation behaviour: as a result of magnetostriction effects, the variation of the sample length can produce variations in the magnetization of the sample, and then the eddy currents appear as a result of the movement of the domain walls. Eddy currents can be referred as Macroeddy currents (flow in a path related to the macroscopic geometry and size of the sample) and Microeddy currents (related to the local individual domain configuration) [42].

1.4.1. Macroeddy Current Strength and Frequencies

According to Zener [48], the Macroeddy current relaxation yields a discrete frequency spectrum composed, in terms of the logarithmic decrement δ, of a sum of simple Debye-like relaxation peaks with characteristic frequencies f_j and heights p_j:

$$\delta_M = \pi \Delta_E^M \sum_{j=1}^{\infty} p_j \frac{f/fj}{1 + \left(f/f_j\right)^2} \quad , \tag{1.3}$$

where f is the frequency of measurements, Δ_E^M is the Macroeddy relaxation strength.

A restriction imposed on p_j is:

, (1.4)

Δ_E^M was defined by Zener [46] using the following equation:

$$\Delta_E^M = \frac{E_U - E_R}{E_R} , \quad (1.5)$$

where E_U and E_R are the values of YM in unrelaxed and relaxed states, respectively.

In terms of magnetic and elastic properties of material, the macroeddy relaxation strength is given by:

$$\Delta_E^M = \frac{E_U}{\mu_0 \mu_r} (\partial B/\partial \sigma)_H^2 , \quad (1.6)$$

where μ_r is the reversible permeability, μ_0 is the permeability of free space and $(\partial B/\partial \sigma)_H^2$ is the differential inverse magnetostriction [39, 42, 45].

Δ_E^M varies substantially with the magnetization of the sample with a maximum value at some intermediate state of M, and becoming zero for both demagnetized and saturation states due to the zero value of at saturation and in demagnetized condition.

On the other hand, the ΔE-effect, in terms of Young Modulus is:

$$\left(\frac{\Delta E}{E}\right)_{mag} = \frac{E_U - E}{E} \quad (1.7)$$

A comparison between (1.5) and (1.7) shows that the maximum value of Δ_E^M is the value of the ΔE-effect. The frequency dependence of Macroeddy ΔE-effect is also typical for relaxation:

$$\left(\frac{\Delta E}{E}\right)_M = \Delta_E^M \sum_{j=1}^{\infty} p_j \frac{1}{1+\left(f/f_j\right)^2} \tag{1.8}$$

Only the first term in the discrete spectra will be taken into account (j=1) to simplify the analysis of the results obtained. This implies that:

$$\begin{cases} p_1 = 1 \\ p_j = 0, \ \ j > 1 \end{cases} \tag{1.9}$$

Consequently, equations (1.3) and (1.8) are reduced to the expressions:

$$\delta_M = \pi \Delta_E^M \frac{f/f_M}{1+\left(f/f_M\right)^2} \tag{1.10}$$

$$\left(\frac{\Delta E}{E}\right)_M = \Delta_E^M \frac{1}{1+\left(f/f_M\right)^2} \tag{1.11}$$

We exclude the high frequency components of Macroeddy relaxation and damping since they do not affect in a major way our present study. Moreover, for our experimental procedure, if j=1, the relaxation frequency of the Macroeddy component can be estimated from the solution for longitudinal oscillations of a circular rod of radius R:

$$f_M \approx \frac{\rho}{\mu_0 \mu_r R^2} \tag{1.12}$$

where ρ is the electric resistivity.

1.4.2. Microeddy Current Strength and Frequencies

Microeddy current relaxation follows the same Debye law introduced for the Macroeddy current damping. Similar to the Macroeddy relaxation, we define the Debye equations for Microeddy relaxations as:

$$\delta_\mu = \pi \Delta_E^\mu \frac{f/f_\mu}{1 + \left(f/f_\mu\right)^2} \tag{1.13}$$

$$\left(\frac{\Delta E}{E}\right)_\mu = \Delta_E^\mu \frac{1}{1 + \left(f/f_\mu\right)^2} \tag{1.14}$$

However, the relaxation strength caused by Microeddy current relaxation is determined by a new set of parameters:

$$\Delta_E^\mu = A \frac{\mu_0 \mu_i \lambda_s E_U}{I_s}, \tag{1.15}$$

where A is a numerical factor, $\mu_i \approx \mu_r$ represents the initial permeability, λ_s is the saturation magnetostriction, and I_s is the spontaneous magnetization. The field

dependence of the relaxation strength of the Microeddy term differs from the Macroeddy one. Δ_E^{μ} is the highest in the demagnetized state and falls to zero at saturation [43, 47].

The frequency of the Microeddy current relaxation can be obtained similar to Eq. (1.12), but with the Radius *R* replaced by the width of the characteristic magnetic domain l [41, 43, 47]:

$$f_{\mu} \approx \frac{\rho}{\mu_0 \mu_r l^2} \tag{1.16}$$

2. Material and experimental technique

2.1. Sample preparation

The Ni_2MnGa crystal that we studied was grown at AdaptaMat Ltd., Finland, using directional solidification. The crystal was homogenized for 96 h at 1300 K and slowly cooled (50 K/h), ensuring Heusler-type atomic ordering and minimizing defect formation. The specimen 1 × 1.1 × 7 mm^3 was spark cut along the [100] direction, ground, and electropolished.

The phase transformation temperatures were determined by means of 4 wire alternating current (ac) impedance measurements at a frequency of 68.6 Hz. The real R and imaginary X parts of the impedance were determined by means of an EG&G 5208 lock-in amplifier, using the electric current across the sample of 6 mA root mean square value.

The ac impedance Z is given by:

$$Z = R + iX \tag{2.1}$$

At low enough frequencies, when the skin effect can be neglected (as in case of the frequency used of 68.6 Hz), the direct current resistivity of materials is directly determined from the R using the law of Ohm. The imaginary part, X, was estimated from the solution for a cylindrical sample:

$$X = \omega L = \frac{\mu l}{8\pi} \tag{2.2}$$

where L is the inductance of the sample, expressed as a function of its permeability and length l.

Thus, Eq. (2.1) and (2.2) allowed us to derive the resistivity and permeability of the sample material.

ρ and μ of the sample versus temperature are shown in Fig. 2.1. In Fig. 2.1 we can see how the phase transformation temperatures are detected in the resistivity and magnetic permeability data. The alloy presents the Curie temperature TC ≈ 383 K, premartensitic transformation temperature TPM ≈ 261 K, and the start temperatures of the direct and reverse martensitic transformations Ms = 201 and As = 206 K, respectively.

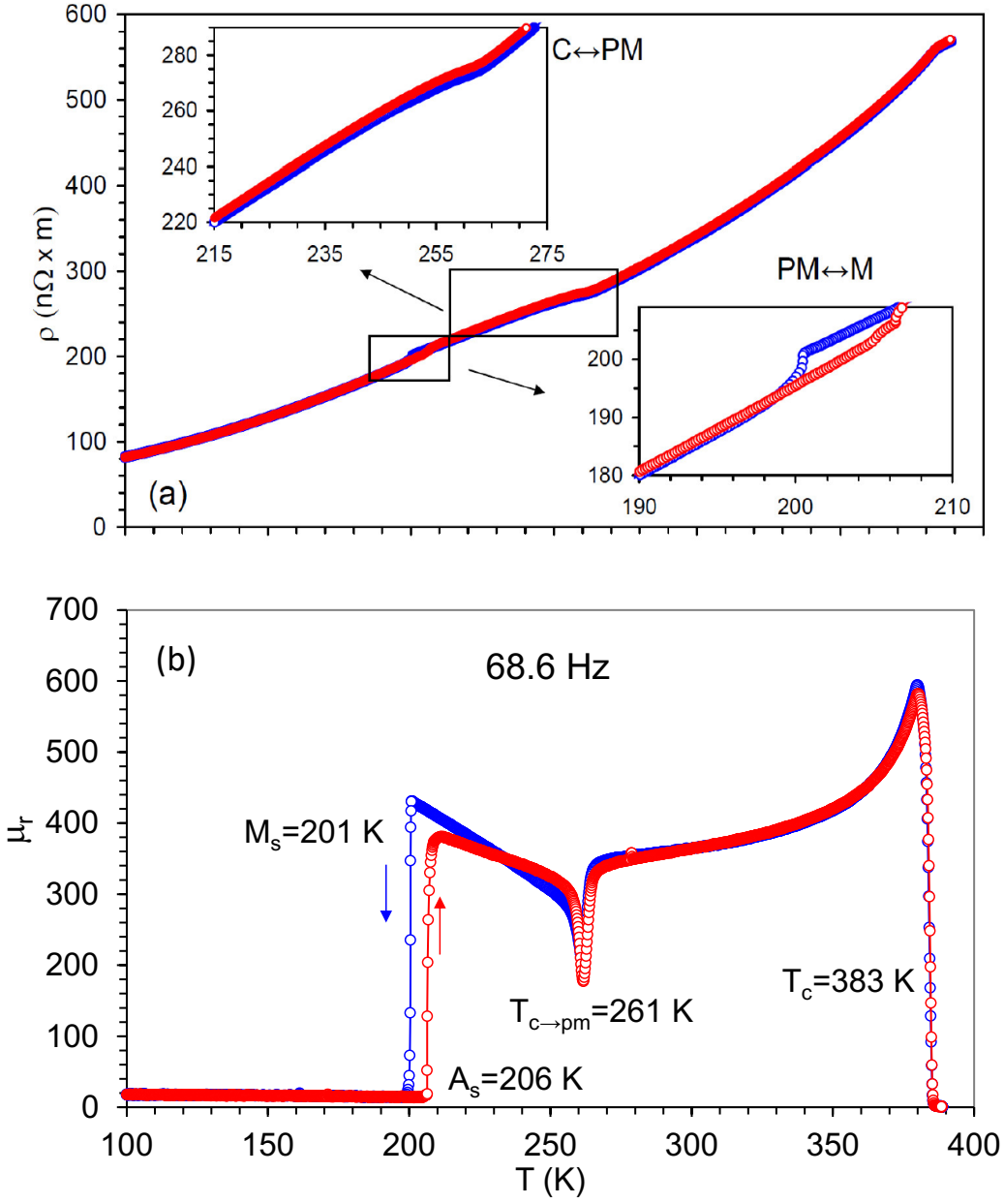

Figure 2.1: Temperature dependence of resistivity (a) and reversible permeability (b) for a sample of [100] oriented Ni2MnGa crystal determined from AC impedance measurements at a frequency of 68.6 Hz

2.2. Experimental procedure

The temperature dependences of the internal friction (IF) and Young´s modulus (YM) at ~90 kHz were studied using the Piezoelectric Ultrasonic Composite Oscillator Technique (PUCOT), which has been traditionally used for the measurements of elastic and anelastic properties at frequencies between 70-140 kHz [42]. A home-made computer-controlled experimental setup [47] operating under Labview software was used. .

The composite oscillator consisted of the Ni_2MnGa sample, cemented to two identical 18.5° x-cut α-quartz crystals of rectangular cross section, plated with electrodes on two sides and supported in their centres (for excitation of the fundamental nodes of longitudinal oscillations) [48]. Figure 2.2 shows that the behaviour of the transducer with increasing strain amplitude ε_0 remains essentially linear: the non-linearity does not exceed 1% up to the strain amplitudes close to 10^{-4}. The overall damping of the quartz also remain low, much lower than the damping measured in a composite oscillator with the sample attached. That means that the contribution of the transducer alone to the measured damping of the sample and transducer remains low and the precision of the determination of the damping of the sample is high.

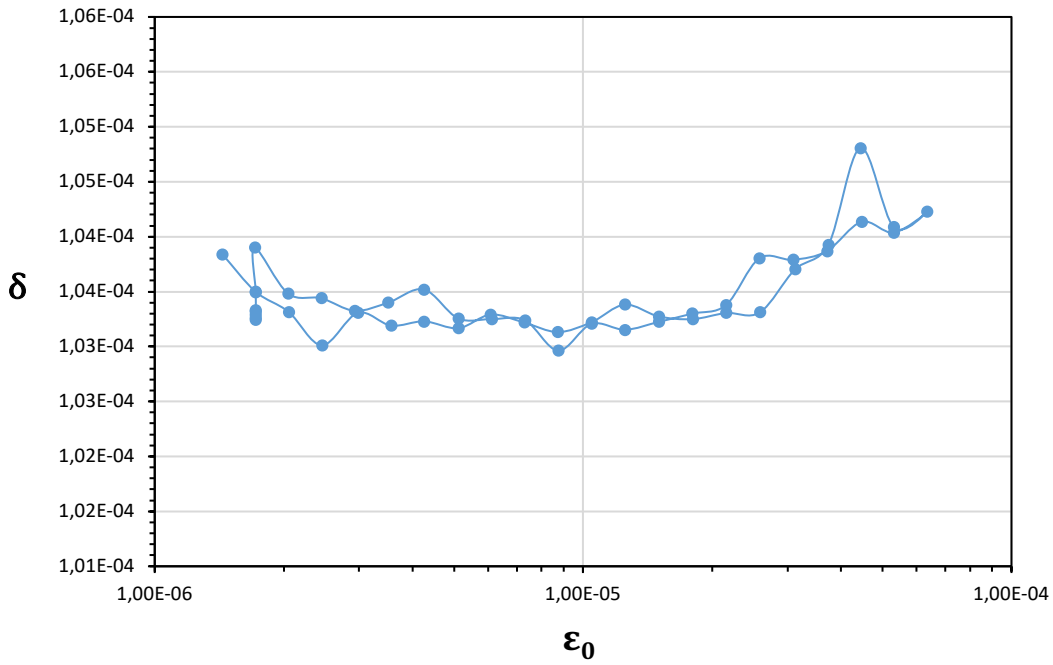

Figure 2.2: Total decrement (δ) of the α-quartz crystal versus strain amplitude (ε_0) at room temperature.

The mechanical oscillations of frequency "f " can be used to obtain information about the microstructure of the material without causing any damage, interacting with the solid to obtain the mechanical energy absorbed [40]. The measurements of internal friction allow us to obtain mechanical loss spectra in function of temperature, or in function of the oscillatory strain amplitude at a constant temperature.

The expressions of damping δ and strain amplitude of the composite oscillator in terms of ac voltages across drive and gauge crystals, U_d and U_g, respectively, were obtained by Robinson and Edgar [48]:

$$\delta = K_\delta \frac{U_d}{U_g}, \tag{2.3}$$

$$\varepsilon_0 = K_\varepsilon U_g, \tag{2.4}$$

where K_δ and K_ε are coefficients.

The damping δ and the resonant frequency f of the specimen are usually obtained from the damping and resonant frequency of the entire composite oscillator δ_c and f_c, and the damping δ_q and frequency f_q of the quartz transducer alone from the equations similar to the rule of mixture:

$$m_c\delta_c = m_q\delta_q + m_s\delta, \tag{2.5}$$

$$m_c f_c = m_q f_q + m_s f \ , \tag{2.6}$$

where m_c , m_q and m_s are the total mass of the composite oscillator, the mass of the quartz transducer alone and of the sample, respectively.
Solving Eq. (2.5), one obtains the damping of the sample as:

$$\delta = \frac{m_c\delta_c - m_q\delta_q}{m_s}. \tag{2.7}$$

Equation (2.7) shows that if the damping of the quartz transducer is much lower than that of the sample, the damping of the sample is determined with high precision [48].

In the present work very strong variations of the Young´s modulus and resonant frequency of the sample were found close to the T_{PM} temperature. Therefore, instead

of using approximate simplified solution (2.6) for the resonant frequency of the sample *f,* more precise solution [50, 51] was used, which requires solution of a transcendental equation:

$$m_q f_q \tan\frac{\pi f_c}{f_q} + m_s f \tan\frac{\pi f_c}{f} = 0 \tag{2.8}$$

Using the numerical values of the resonant frequency of longitudinal oscillations of the rod-shaped sample from the solution of Eq. (2.8), the Young´s modulus was derived as:

$$E = 4\rho f^2 l_1^2 \tag{2.9}$$

The control software was based on LabView package. During the measurements of the strain amplitude dependences, the IF, resonant frequency and strain amplitude were measured simultaneously as a function of time. During registration of the temperature dependences, first, the strain amplitude of oscillations was stabilized at a pre-selected value in each temperature point. After stabilization, the IF and resonant frequency of the oscillator was measured. Moreover, the control software allowed us to measure the strain amplitude dependence of the decrement and resonant frequency at any point of the temperature spectra, using interruptions of the temperature spectra measurement. After measurements, the system re-engaged the registration of the temperature spectra [48].

The advantages of the system regarding other piezoelectric techniques used in previous experiments (see [50, 53, 54]) are as follows [48]:

1. Adaptive measurement procedure, when the time–resolution depends upon current values of registered absorption of ultrasound.

2. Automatic selection of an appropriate measurement range.

3. Combined analog-digital control of drive-voltage (strain amplitude) which substantially simplifies the electronics design

4. Resonant conditions for oscillations, checked and maintained at each measuring point quite rapidly owing to a procedure of polynomial fitting of the resonant curve.

5. Wide application of highly integrated high-precision analog circuits instead of digital ones, resulting in simple and compact design.

Regarding the study in case, the procedure owns a variety of advantages, inherent in this acoustic method [48]:

1. Measurements cover a wide range of damping and strain amplitude: no mechanical parts are involved, resulting in a low level of background damping.

2. Fast measurements: important for studying the transient phenomena.

3. Simple and accurate: in practice, only two voltages across transducers need to be measured.

4. Detailed: Practically continuous curves of damping or modulus versus strain amplitude can be registered.

5. Resonant conditions can be easily maintained: positive feedback in closed-loop configuration holds the oscillator at resonance.

The temperature range studied was between 245 and 300 K, covering the range of the PMT. To demagnetize the sample, it was heated above the Curie temperature, up to 393 K. The polarizing magnetic field H had uniformity better than 0.5% in the working space containing the sample. The magnetic field was created by means of a 400mm-long, 60mm-diameter solenoid placed around the cryostat. Figure 2.3. shows the photo of the cryostat with the solenoid.

The homogeneity of the true magnetic field inside the Ni_2MnGa sample was deteriorated by demagnetizing effects, and the values of true field are difficult to compute. However, the sample was rather long in the direction of applied field compared to its transverse dimensions. This allowed us to consider demagnetizing factor small enough.

To estimate the demagnetizing factor, the sample was considered as an ellipsoid with axial ratios of 7: 1.1: 1.0. Then, for the field applied along the rectangular bar-shaped sample, the demagnetizing factor is around 0.04 [55].

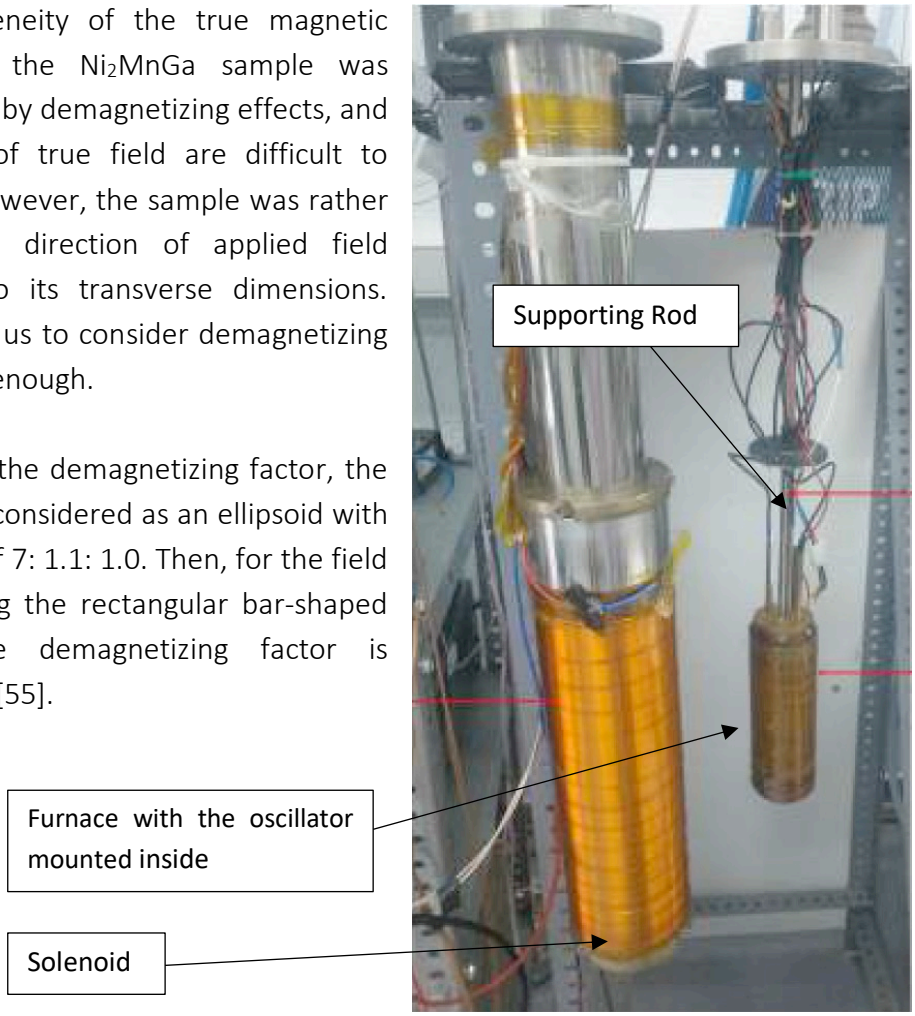

Figure 2.3. The photo showing the cryostat with mounted solenoid and the interior of the cryostat consisting of the supporting rod and copper furnace with the oscillator inside.

3. Results: Analysis

3.1. Temperature dependence of the internal friction and Young´s modulus

Figure 3.1 shows temperature dependence of the internal friction and Young´s modulus for demagnetized state of the sample and under applied field H=9 kA/m and 18 kA/m. Measurements were taken during cooling and consequent heating of the sample down to 245 K, well below the temperature of premartensitic transformation, $T_{PM} \approx 260$ K, but well above the temperature of the martensitic transformation, M_s=201 K.

3.1.1. Demagnetized State

Data in Fig. 3.1(a) indicate the existence of the IF peak during premartensitic transformation. The IF shows the temperature hysteresis of the PMT peaks of 0.5-1.0 K, which is in agreement with the permeability data, shown in Fig 2.1. This IF hysteretic behaviour is observed even after several thermal cycles, and, therefore, is not related to potential gradual structural modifications of the material during thermal cycling. Thus, the small hysteresis confirms weak first order nature of the PMT.

Another characteristic feature of the PMT is a double IF peak and YM minimum, most clearly seen in the demagnetized state. Still, the high-temperature component of the double IF peak and YM minimum is seen as a shoulder under polarizing fields of 9 and 18 kA/m. Similar splitting of the IF peak during PMT was observed by Seiner et al. [14].

The third peculiarity is notably higher IF level in the cubic phase during heating from below PMT than in the demagnetized state (during cooling from above Tc). A comparison of Fig. 3.1(a) and 3.1(b) shows that this hysteresis of the IF is not accompanied by a detectable YM variation, however. The demagnetized low IF level is recovered after heating the sample above Tc.

The reason for the higher values of the IF in the cubic phase during heating from below the PMT temperature than in the demagnetized state is the increase of the Microeddy current damping due to the modification of the magnetic domain structure during the PMT, more specifically, the increase of the average domain size and decrease of the Microeddy relaxation frequency [37].

Since the microeddy current relaxation process is relaxed ($f_0 << f_\mu$), the detectable variation of the IF is accompanied by very small, undetectable variation of modulus defect. Therefore, the modulus is much less sensitive to the variation of relaxation frequency than the IF and the modulus curve does not show hysteresis.

YM values depicted in Fig. 3.1(b) are in good agreement with previous data on C', obtained by RUS at the same temperature and frequency ranges [9, 24, 55].

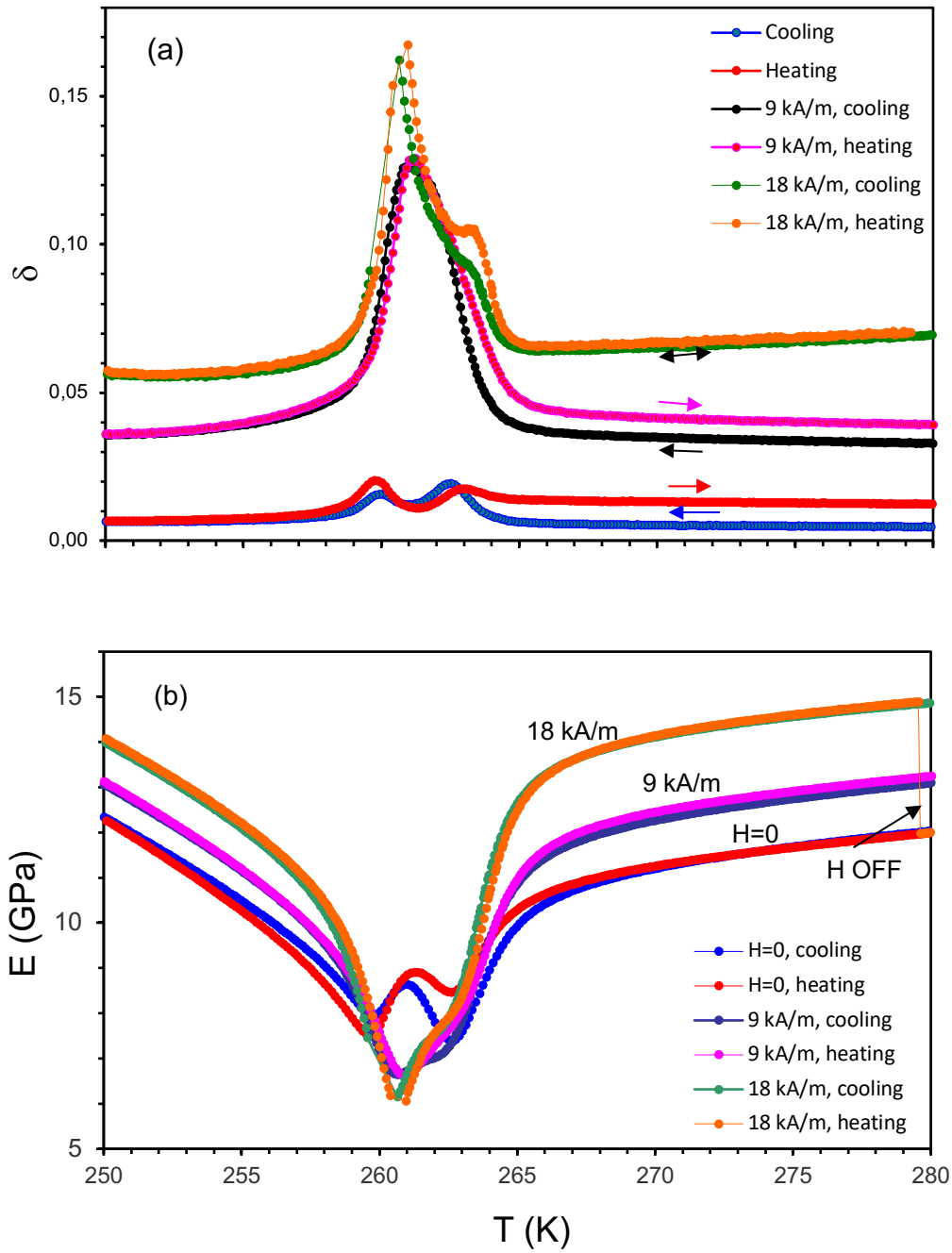

Figure 3.1: Internal friction (a) and Young´s modulus (b) temperature spectra under cooling and heating for the demagnetized sample and under magnetic fields of 9kA/m and 18kA/m for a cooling-heating rate of 0.5ºK/min and an oscillatory strain amplitude of $2x10^{-7}$. The effect of removal of the applied field of 18kA/m on the Young´s modulus value in the cubic phase during heating is marked as H OFF.

3.1.2. Moderate Fields

Measurements under 9 kA/m and 18 kA/m show a substantial increase of damping both outside the PMT range and during the transformation, Fig. 3.1(a). The IF during the PMT reaches a value 15 times higher than in the demagnetized state. Moreover, the IF constantly escalates with H in the premartensitic phase (at $T<T_{PM}$), which is similar to the effect observed in [38].

The effect of magnetic field on the YM, Fig. 3.1(b), is quite different and more complicated, however. The YM increases under field outside the PMT range (whereas the IF also increases), but softens during the PMT. Thus, the effect of moderate applied field on the YM is opposite in the cubic and premartensitic phases and during the PMT.

Second, we notice that the IF hysteresis in the cubic phase between cooling and heating decreases at 9 kA/m and totally disappears at 18 kA/m. This observation is in line with the suggested interpretation of this hysteresis as due to variation of the magnetic domain size during PMT: sufficiently high applied field makes the effect of PMT on the variation of the domain size negligible.

The effect of H=18 kA/m field removal on the YM in the cubic phase is shown in Fig. 3.1(b). This experiment shows that the YM immediately recovers the values practically coincident with those for the demagnetized state.

3.2. Strain amplitude dependence of the internal friction and resonant frequency.

The reason for studying strain amplitude dependence of the IF and YM is a possibility to observe and study separately the linear and non-linear anelastic effects, normally having different microscopic origins. In the case of magnetomechanical damping the linear components are micro- and macroeddy current relaxations, the non-linear term is the hysteretic magnetomechanical damping.

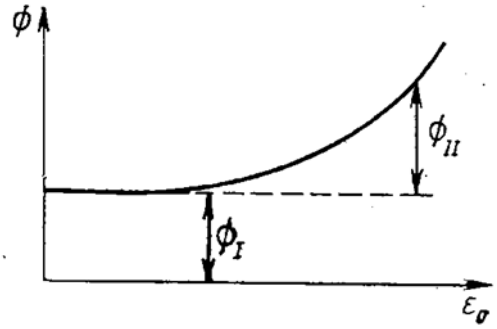

Figure 3.2. Schematic representation of the strain amplitude dependence of the total internal friction Φ and its separation into the linear low-amplitude background Φ_1 and non-linear high-amplitude term Φ_2 [41].

Figure 3.2 [41] shows schematically a typical strain amplitude dependence of damping Φ. The linear (independent on strain amplitude ε_0) IF background is usually observed at low oscillatory strain amplitudes. At higher strain amplitudes the IF becomes dependent on strain amplitude. A classic approach is to consider the linear and non-linear IF components as additive (independent). Then, following classical textbook by Nowick and Berry [39], the total damping is written as a sum of linear and non-linear terms:

$$\Phi = \Phi_I + \Phi_{II} \tag{3.1}$$

Expressing the IF in terms of the logarithmic decrement, accepted in the present work, we define the total IF $\delta_{tot}(\varepsilon_0)$ as a sum of linear, strain amplitude independent, δ_i and strain-amplitude dependent non-linear $\delta_h(\varepsilon_0)$ terms:

$$\delta_{tot}(\varepsilon_0) = \delta_i + \delta_h(\varepsilon_0) \tag{3.2}$$

In the present results the non-linear IF term was determined using Eq. (3.2) as:

$$\delta_h(\varepsilon_0) = \delta_{tot}(\varepsilon_0) - \delta_i \tag{3.3}$$

Thus, the linear IF term is directly measured experimentally as a low-amplitude background, whereas the non-linear IF term is determined for each strain amplitude dependence as a difference between the total damping and low-amplitude background.

In order to obtain more information about the complex IF and YM patterns close to PMT, we have studied the dependences of the sample frequency f and of the total

damping δ_{tot} versus strain amplitude ε_0 at several key temperatures before (289.7 K), after (249.8 K) and during the premartensitic transition (259.9/262.9 K).

To this end, the temperature dependence measurements were interrupted during the cooling/heating cycles, and several strain amplitude dependences of the IF and of resonant frequency at constant temperatures but under different polarizing fields were carried on. In other words, the effect of applied field on the strain amplitude dependence of the IF and resonant frequency was studied in three temperature domains: in the cubic and premartensitic phases and over the PMT temperature range.

Four measurements were taken for each temperature at each value of the magnetic field. We performed measurements of the strain amplitude dependences for 15 values of increasing and 15 values of decreasing field between 0 and 18kA/m. Of the total of 4 measurements for each filed, the first two measurements were performed when increasing the magnetic field, whereas the other two measurements were on the decrease of the field. The first measurements under both increasing and decreasing fields always showed irreversibility between increasing and decreasing strain amplitudes (or so-called strain amplitude hysteresis). The second consecutive measurement yielded perfectly reproducible strain amplitude dependences. The existence of the hysteresis in the first measurement is a very interesting phenomenon, which we attribute to the metastable configurations of the domain walls after increasing/decreasing H. An additional excitation of the domain walls by periodic oscillatory stress during the first measurement triggers the domain wall motion towards deeper energy minima. These positions remain the same in the second measurement of the strain amplitude dependence. Here we present the results of the second measurements (taken on the second time for rising the magnetic field).

In the cubic phase, at 289.7 K, the results obtained show a monotonous increase of the frequency, Fig. 3.3(a), and IF Fig. 3.3(b) versus magnetic field. The values of internal friction reach a maximum of δ=0.08 when H=18kA/m, which are in agreement with the ones obtained in the temperature dependence experiments. The values of frequency are between 100-110 kHz, close to the frequency range of macroeddy current relaxation, Chapter 2. We were not able to reach the saturating magnetic field. However, we can observe a decrease of the strain amplitude-dependent decrement (for example, for the strain amplitude above $\varepsilon_0=10^{-5}$). Panel (c) depicts the non-linear component δ_h.

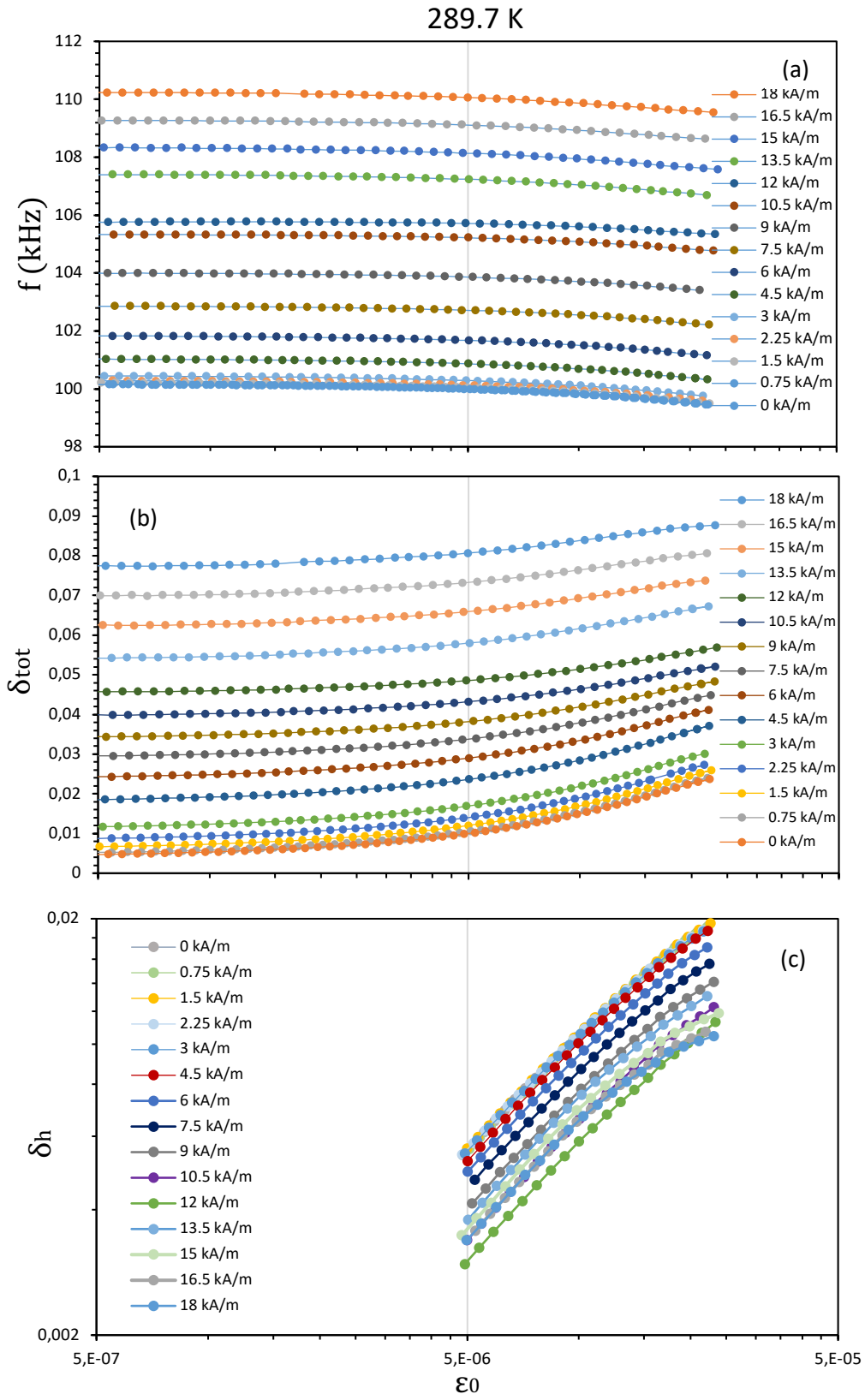

Figure 3.3: Sample frequency (a) and total decrement δ_{tot} (b) and non-linear decrement δ_h (c) versus strain amplitude at 289.7K in the demagnetized state (H=0) and under different magnetic fields H, indicated by numbers (in kA/m) close to each curve. Experimental points correspond to increasing strain amplitude scans.

The data obtained at 249,8 K (Fig. 3.4) are qualitatively similar to the ones registered at 289.7 K. Nevertheless, a somewhat lower non-linear IF term is found in the premartensitic phase, below the T_{PM}. The suppression of the non-linear component of the IF by applied field is also observed in the premartensitic phase.

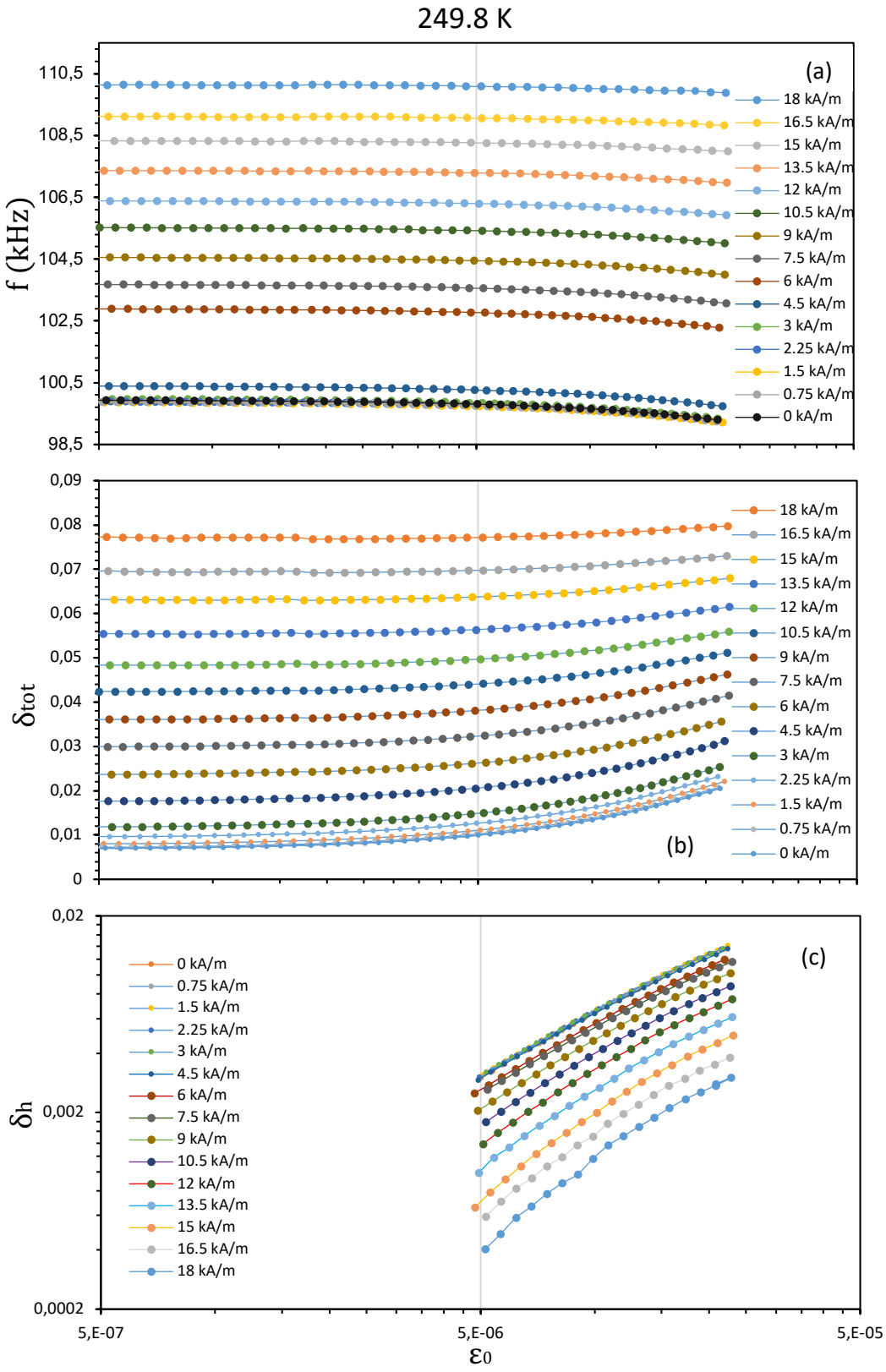

Figure 3.4: Sample frequency (a), total decrement δ_{tot} (b) and non-linear decrement δ_h (c) versus strain amplitude at 249.8K in the demagnetized state (H=0) and under different magnetic fields H, indicated by numbers (in kA/m) close to each curve. Experimental points correspond to increasing strain amplitude scans.

Measurements at 259.9 K, Fig. 3.5, are close to the second IF peak of the demagnetized state during cooling the sample. The IF values were too high at this temperature to scan the same range of the strain amplitudes as in the cubic and premartensitic phases. In addition, we could not rise the magnetic field up to 18 kA/m, instead of that we could reach only 12kA/m. However, we can clearly observe the behaviour of the linear and non-linear IF components. Figure 3.5(b) shows a strong increase of both linear and non-linear IF terms. However, the most remarkable is a qualitatively different effect of applied field on the resonant frequency of the sample (Young´s modulus). We note that whereas the application of field resulted in the modulus increase in the cubic and premartensitic phases (Figs. 3.3(a), 3.4(a)), the resonance frequency decreases (modulus softens) under field in the temperature range of the PMT, Fig. 3.5(a). The decrease of the frequency during PMT is consistent with the behaviour of the temperature spectra shown in Fig. 3.1(b).

Another important effect in the data of Fig. 3.5(c) is a much stronger suppression of the non-linear damping at 12 kA/m than in the cubic and premartensitic phases and slowing down of the δi increase under 12 kA/m.

The temperature T=262.9 K corresponds to the high-temperature side of the high-temperature component of the double IF peak in the demagnetized state. According to Fig. 3.6, the effect of applied field on resonance frequency recovers the trend typical for the cubic and premartensitic phases, i.e., the frequency increases under field, Fig. 3.6a. At the same time, the IF vs strain amplitude curves show different trend compared to other temperature points studied, Fig. 3.5b. As in figures 3.3, 3.4 and 3.5, at low amplitude ε_0=5x10^{-7}, the IF increases monotonously when intensifying magnetic field. However, the decrease of the non-linear component of damping is much more intense starting from the smallest values of applied field. As a consequence, the ***total damping*** at high strain amplitudes shows a maximum (whose position against field depends on the strain amplitude) and then drops rapidly. The intense decline of the non-linear damping by field is concomitant with a suppression of the strain amplitude dependence of the resonant frequency. The strong suppression of the non-linear effects and saturation of the low-amplitude background increase under field indicate that at T=262.9 K we are getting closer to the saturating field than in the premartensitic and cubic phases and during the PMT at T= 259.9 K.

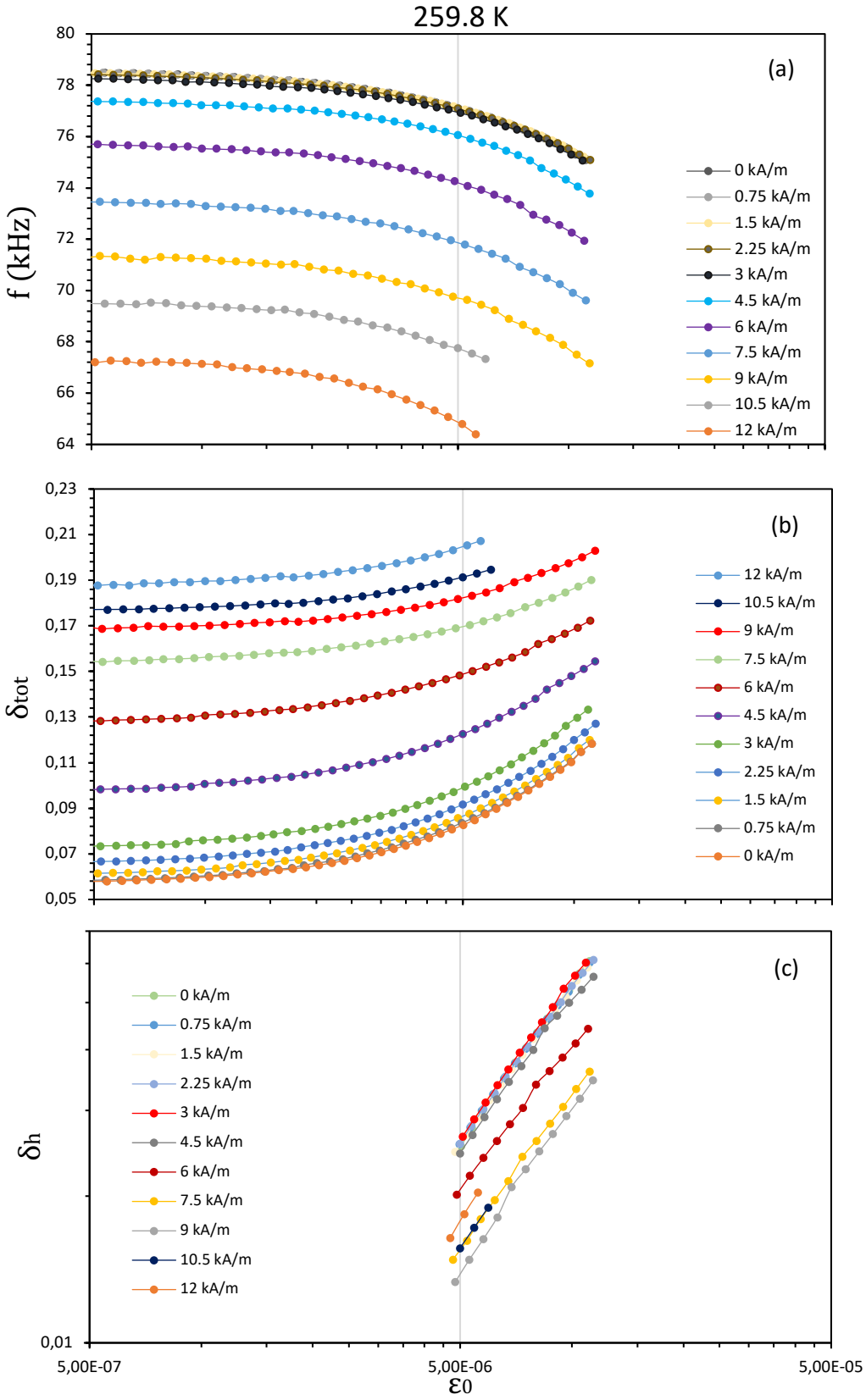

Figure 3.5: Sample frequency (a), total decrement δ_{tot} (b) and non-linear decrement δ_h (c) versus strain amplitude at 259.5K in the demagnetized state (H=0) and under different magnetic fields H, indicated by numbers (in kA/m) close to each curve.

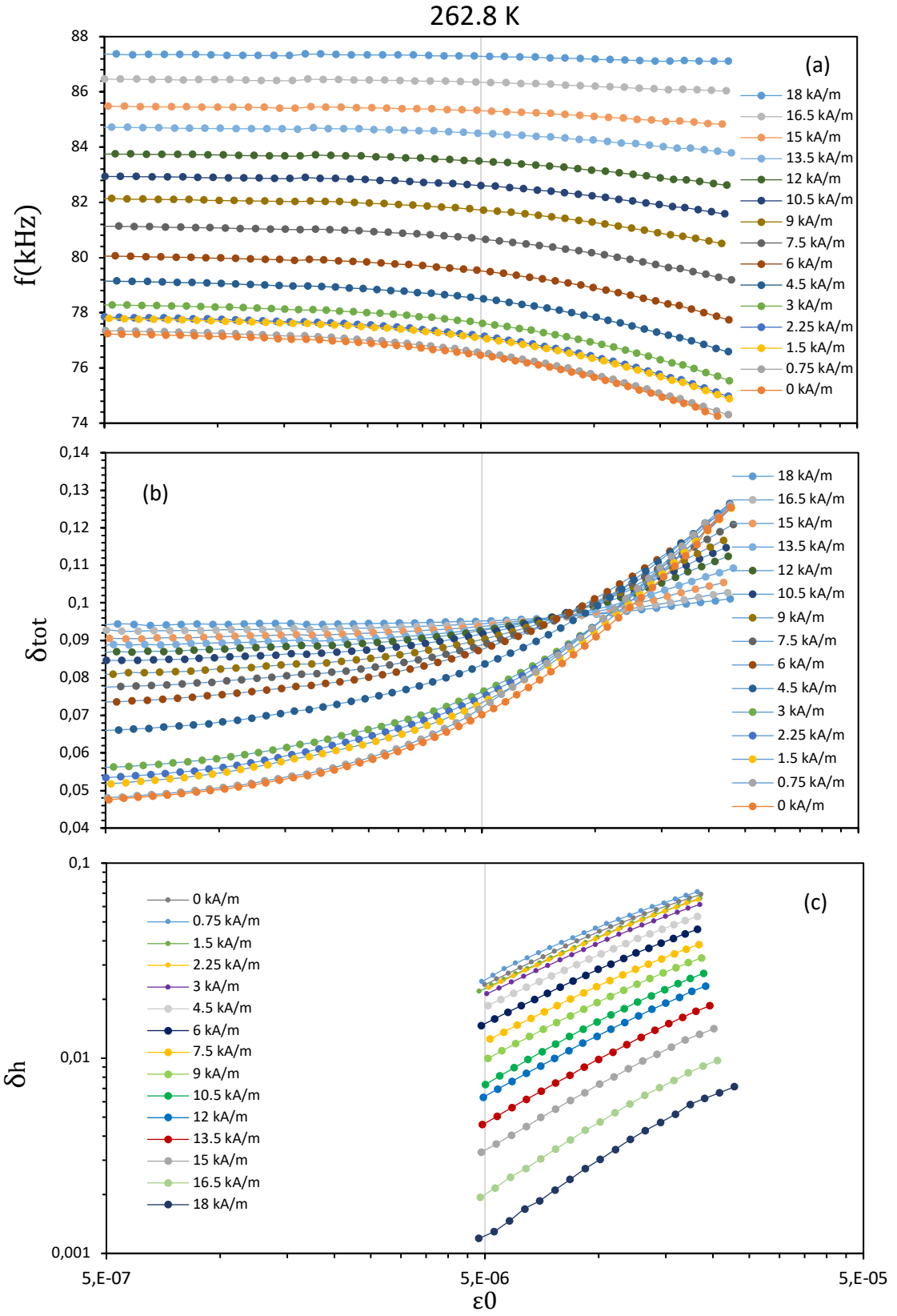

Figure 3.6: Sample frequency (a), total decrement δ_{tot} (b) and non-linear decrement δ_h (c) versus strain amplitude at 262.85K in the demagnetized state (H=0) and under different magnetic fields H, indicated by numbers (in kA/m) close to each curve.

3.3. Applied field dependences of the internal friction and Young´s modulus

Field dependences at different fixed temperatures of the linear and non-linear components of the IF and of the YM (recalculated from the resonance frequency) are shown in Fig. 3.7. These plots are derived from the strain amplitude dependences shown in Figs. 3.3-3.6. The values of the non-linear damping correspond to the strain amplitude $\varepsilon_0 = 5x10^{-5}$ for temperatures 289.7, 249.8 and 262.9 K and to $\varepsilon_0 = 5\text{x}10^{-6}$ for T=259.9 K.

Results obtained for 289.7 K and 249.8 K (in the cubic and premartensitic phases, respectively) represent opposite tendencies in the linear damping and Young modulus: the IF increases continuously with field, whereas the YM hardens. δ_h is continuously supressed by H, reaching values close to zero, indicating approaching to the saturating field. We can observe a similar behaviour of δ_i and YM for the PMT range 262.9 K, with a more intense suppression of DW-related δ_h. This anomalous behaviour of the linear components of the modulus defect and internal friction has been analysed for the cubic phase in Ref. [38]. In principle, the opposite effect of applied field on the IF and YM can be explained by an extremely intense shift of the microeddy relaxation peak to lower frequencies under field. However, quantitative estimations made in [38] suggest another scenario, involving both micro- and macroeddy current relaxations. More specifically, the IF measured at f ~10^5 Hz increases in a conventional way under the non-saturating field due to the net magnetization of the sample, producing a macroeddy current IF. At the same time, the YM is hardened because of the suppression of the microeddy current ΔE-effect, which is predominant as compared to macroeddy ΔE-effect in the cubic phase at the measuring frequency, which is much lower than the frequency of microeddy current relaxation in the cubic phase (close to 5-10 MHz) [37].

However, this pattern changes in the data at 262.9 K where the increase of damping is accompanied by a decrease of the modulus. Thus, the unusual behaviour of the IF and YM explained by the simultaneous involvement of both micro- and macroeddy current relaxations, changes to the one, typical for conventional macroeddy relaxation. Thus, one has to explain this change of the IF and YM pattern by variations of the micro- and macroeddy relaxation parameters during the PMT.

In summary, the experimental observations that need to be explained are as follows:

- The internal friction peak versus temperature during the PMT;
- Splitting of this peak into two components, which is concomitant with the double minimum of the Young´s modulus;
- Switching between the unusual opposite tendencies in the field dependences of the internal friction and Young´s modulus, observed in the cubic and premartensitic phases, to the tendency typical for a conventional relaxation over the narrow temperature range close to the PMT.

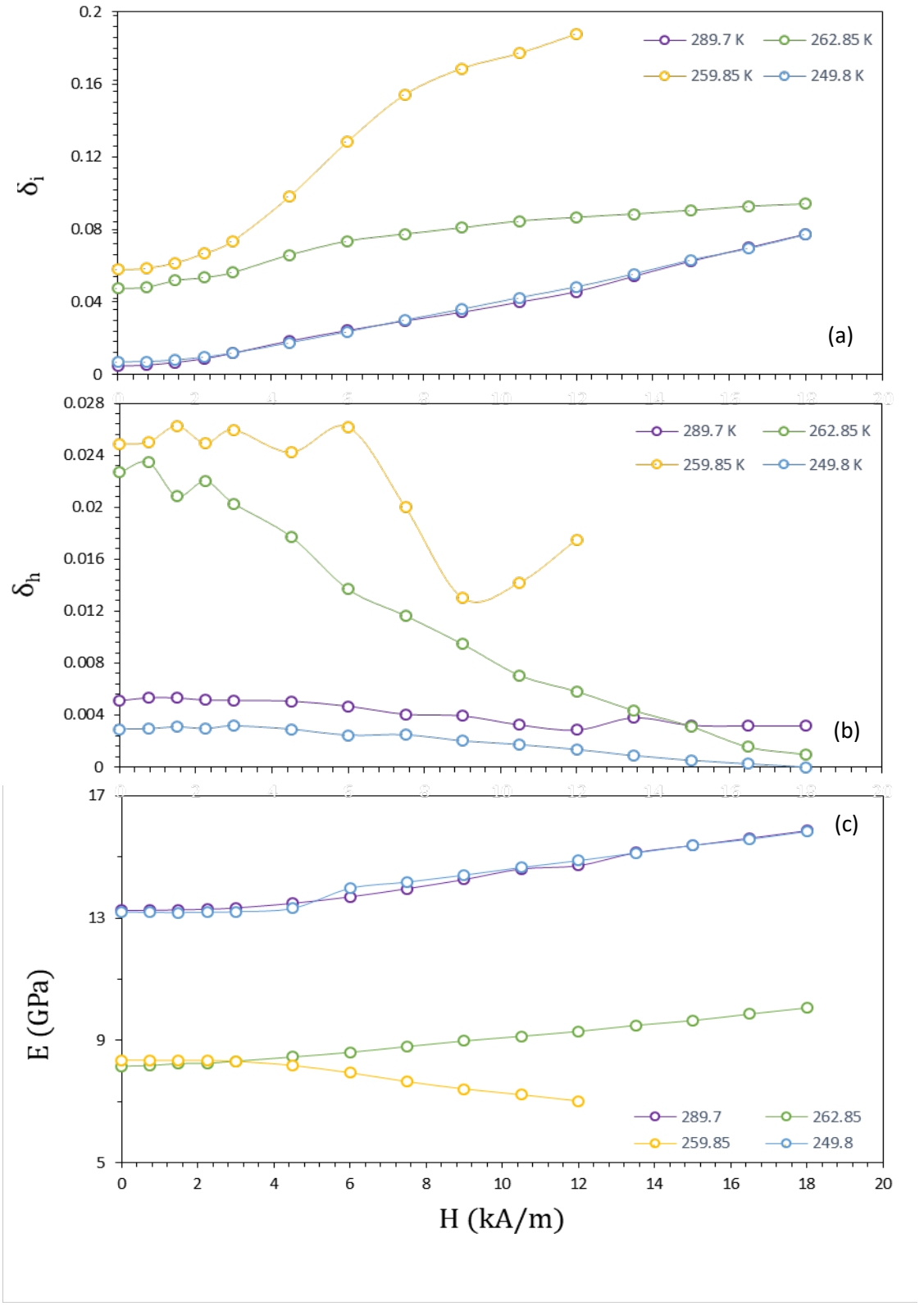

Figure 3.7: Linear (a) and non-linear (b) components of decrement, δ_i and δ_h, respectively, an Young Modulus (c) versus field H at 289.7 K, 249.5 K, 262.15 K and 259.7 K. Values of δ_i corresponds to a low-strain amplitude of $\varepsilon_0=5x10^{-7}$ for all temperatures, whereas the values of δ_h are related with values of $\varepsilon_0=5x10^{-5}$for 289.7 K, 249.5 K, 262.15 K and $\varepsilon_0=5x10^{-6}$ for 259.7 K.

4. Interpretation of results

4.1. Frequency and field dependence of micro- and macroeddy internal friction and modulus defect

Micro- and macroeddy current relaxation are strongly frequency and applied field dependent. Therefore, first, it is necessary to locate the present results on an appropriate position in the frequency domain. Figure 4.1 shows schematically frequency spectra of macroeddy and microeddy components of the internal friction (a) and ΔE-effect (b). For simplicity, these relaxations are represented by single Debye relaxations, Eqs. 1.10, 1.11 , 1.13 and 1.14. According to the estimations realized in Ref. [38], the frequency of microeddy relaxation, f_μ, is close to (5-10) MHz, whereas the macroeddy current relaxation frequency can be estimated as close to 10 kHz. Therefore, the frequency used in the present experiments f_0 ≈100 kHz is much lower than the microeddy relaxation frequency and is higher than the macroeddy one:

$$f_M < f_0 << f_\mu. \tag{4.1}$$

According to Fig. 4.1, for $f = f_0$ the maximum values (with respect to their field dependence) of the two relevant parameters:

$$\delta_M^{\max} >> \delta_\mu^{\max}, \tag{4.2}$$

$$\left(\frac{\Delta E}{E}\right)_M^{\max} << \left(\frac{\Delta E}{E}\right)_\mu^{\max}, \tag{4.3}$$

since the macroeddy relaxation is unrelaxed at f_0 and has high IF and low modulus defect, while the microeddy current process is relaxed and is characterized by high modulus defect and low IF. We mention also that the maximum values of the

macroeddy relaxation parameters correspond to certain magnetization of the sample (applied field H=Hm), whereas the maximum of the microeddy parameters is reached in the demagnetized state and decline rapidly with the applied field.

Figure 4.2 shows the effect of applied field H on the micro- and macroeddy components of the internal friction and modulus defect for a frequency close to f_0, that is, taking into account the relationships of equations 4.2 and 4.3. It explains the unusual for a single relaxation simultaneous increase of the total linear internal friction (the sum of micro- and macroeddy current components) and decrease of the total modulus defect by the field applied in the cubic and premartensitic phases of material: the internal friction is controlled by the increase of macroeddy current damping component while the modulus defect - by the suppression of the microeddy current modulus defect.

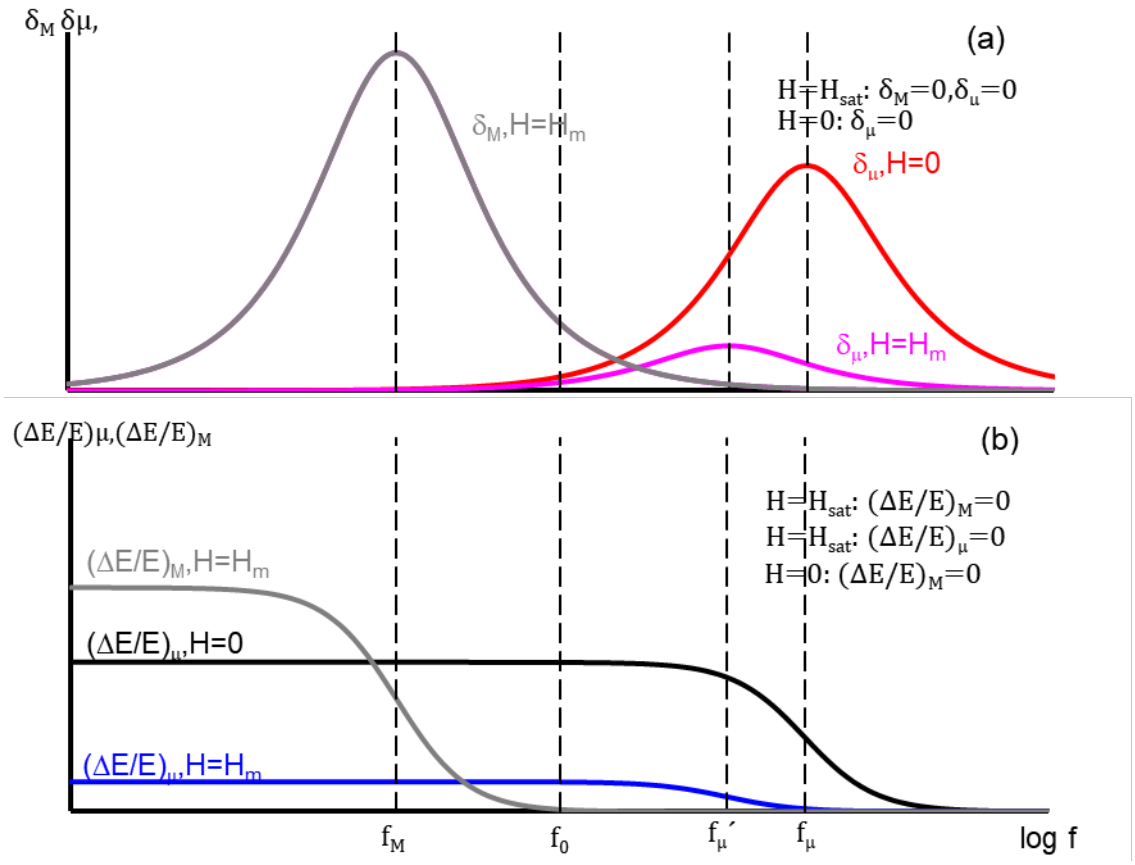

Figure 4.1: Effect of frequency (schematically, note the logarithmic scale) on microeddy $\delta\mu$ and macroeddy δ_M damping components (a) and on the microeddy and macroeddy ΔE-Effect, $(\Delta E/E)_\mu$ and $(\Delta E/E)_M$, respectively. Macroeddy effects are shown for a magnetic field $H=H_m$, corresponding to the maximum relaxation strength, whereas the microeddy effect is shown for the demagnetized state H=0 and under field $H=H_m$, when the macroeddy term is more intense. Dotted lines show the frequencies of the microeddy ($f\mu$) and macroeddy relaxations (f_M). f_0 marks the experimental frequency [38].

This preliminary analysis allows us to explain the three unusual features of the anelastic effects during PMT, listed in Section 3.3. To find the interpretation one needs to analyse the parameters which control the frequency and strength of both micro- and macroeddy current relaxations and to check how these parameters change during the PMT.

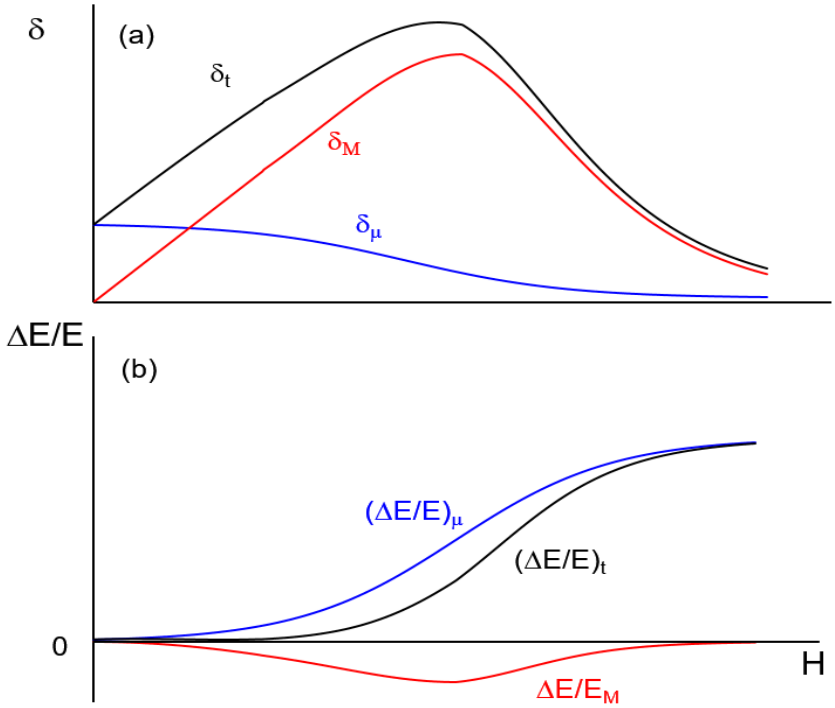

Figure 4.2. Schematic representation of the influence of applied magnetic field H on the micro- and macroeddy current components of damping (a) and modulus defect (b) [38]. a) the microeddy dm and macroeddy dM linear components of the internal friction are shown together with the total internal friction dt, their sum;b) the microeddy $(\Delta E/E)_{\mu}$ and macroeddy $(\Delta E/E)_{M}$ linear components of the modulus defect are shown together with the overall behaviour of the resulting total modulus defect $(\Delta E/E)_{t}$.[37]

4.2. Parameters affecting Microeddy and Macroeddy current relaxations during premartensitic transformation in Ni2MnGa.

Equations 1.6, 1.15, 1.12 and 1.16 from Section 1 yield the relaxation strengths , and frequencies f_M, f_μ of macro- and microeddy current relaxations, respectively. They are reproduced below as Eqs. 4.4-4.7, keeping the original notations of Eqs. 1.6, 1.15, 1.12 and 1.16 Unfortunately, the numerical values of certain parameters in Eqs. 4.4-4.7 remain unknown, making impossible calculations of the absolute values of internal friction and ΔE-effect temperature spectra for both Microeddy and Macroeddy contributions. More specifically, the lack of knowledge of the effects of temperature and magnetic field on differential inverse magnetostriction $(\partial B/\partial\sigma)_H$ for the Macroeddy current relaxation strength Δ_E^M, which impedes the calculation of the $(\Delta E/E)_M$ and the damping δ_M (Eqs. 1.10 and 1.11 of Section 1, respectively). The unknown is the effect of temperature and magnetic field on the magnetic domain structure. Therefore, remains unknown the domain size l, which controls the Microeddy relaxation effects through the relaxation frequency, as is indicated in Eq. 4.6.

Equations 4.4-4.7 show that the main parameters controlling the micro- and macroeddy relaxations, apart from $(\partial B/\partial\sigma)_H$ and l, are: the reversible (or initial) permeability μ_r, the saturation magnetostriction λ_s and the Young´s modulus in the unrelaxed state E_U. Despite the lack of knowledge of $(\partial B/\partial\sigma)_H$ and l, we can analyse qualitatively, and if possible, quantitatively, the influence of μ_r, λ_s and E_U on the frequencies and strengths of eddy current relaxations during the PMT in order to interpret the IF and YM behaviour over this temperature range.

$$\Delta_E^M = \frac{E_U}{\mu_0\mu_r}\,(\partial B/\partial\sigma)_H^2 \tag{4.4}$$

$$\Delta_E^\mu = A\,\frac{\mu_0\mu_i\lambda_s E_U}{I_s} \tag{4.5}$$

$$f_\mu \approx \frac{\rho}{\mu_0\mu_r l^2} \tag{4.6}$$

$$f_M \approx \frac{\rho}{\mu_0\mu_r R^2} \tag{4.7}$$

We will now analyse the variation of the parameters defined by Eqs. 4.4-4.7 during the PMT and, hence, their effects on the micro- and macroeddy relaxations.

4.2.1. Eddy current relaxation frequencies during PMT, Eqs. 4.6 and 4.7.

Figure 2.1(a) indicates that the resistivity ρ remains essentially constant during the PMT, whereas μ_r, Fig. 2.1(b) shows a sharp drop around 50%. Therefore, according to Eqs. 4.6 and 4.7, the frequencies of both Microeddy and Macroeddy relaxations increase sharply during the PMT. However, we mentioned in Section 1.4.2. that after cooling down below PMT the Microeddy relaxation frequency actually decreases, which is due to the variation of the domain size. The latter effect overcompensates the decline of μ_r in f_μ. Therefore, eventually, f_M increases sharply around T_{TPM} but f_μ slightly decreases. Since:

$$f_M < f_0 < f_\mu \ , \tag{4.8}$$

both shifts of the relaxation frequencies make them closer to the f_0 frequency. Therefore, according to Fig. 4.1 and Eq. 1.10 and 1.13, the shift of the relaxation frequencies promotes both micro- and macroeddy current damping components during the PMT, but more notably δ_M. This fact is one of the reasons for the formation of the IF peak during the PMT.

4.2.2. Eddy current relaxation strengths during PMT

The relaxation strengths are defined by Eqs. 4.4 and 4.5 for macro- and microeddy current mechanisms. As mentioned previously, the reversible/initial permeability shows a sharp decline during PMT by approximately one half of its value. We could not determine E_U directly, since the maximum applied field of 18 kA/m in our experiments was below the saturating field. Still, the behaviour of the E_U can be estimated from the C´ elastic constant data ($E_U \approx 3C'$ for cubic Ni-Mn-Ga) reported in Ref. [55]. The C´ under saturating field (and hence the E_U) decreases around 40% during PMT. According to Refs. [23, 57] magnetostriction shows an increase exceeding 2 times, also rather sharp, during PMT.

$\Delta_{\mu} = \frac{\mu_0 \mu_r \lambda_s E_u}{I_S}$	$\Delta_M = \frac{E_U}{\mu_0 \mu_r} \left(\frac{\partial B}{\partial \sigma}\right)_H^2$
- SUPRESSED BY E_U	- SUPRESSED by E_U
- SUPRESSED BY μ_r	- PROMOTED BY μ_r
- PROMOTED BY λ_s	- PROMOTED BY λ_s

Table 1: Effect of the main parameters on the microeddy and the macroeddy relaxation strengths, Δ_{μ} and Δ_M respectively.

Table 1 represents qualitative analysis of the effect of the three crucial parameters, μ_r, λ_s and E_U on the relaxation strengths of micro- and macroeddy relaxations.

We note first that the variation of the E_u reduces the Microeddy and Macroeddy current relaxation strengths around 40% during PMT.The Microeddy relaxation strength, Δ_{μ}, is proportional to the initial permeability $(\mu_i \approx \mu_r)$, saturation magnetostriction(λ_s), and unrelaxed modulus E_U. Therefore, it is suppressed both by E_U (by approximately 40%) and μ_r (by roughly 50%) during PMT, but is promoted more than 2 times by λs. Temperature dependences of μ_r (our data from Fig. 2.1b) and λs [23, 57] over the PMT range are shown in Fig. 4.3. Figure 4.3 shows also their product, which controls the microeddy current relaxation strength. Due to the the opposite behaviour of these parameters during PMT, the product between μ_r and λ_s shows a double maximum versus temperature, with a sharp decline, provoked by the drop in permeability. This is precisely the experimental behaviour of the damping during the PMT, which shows a double peak. As we discussed before, despite the lack of knowledge of E_U, we know that at this temperature E_U drops by around 40%. Therefore, the final value of the Microeddy current relaxation strength could be even lower than in the cubic phase.

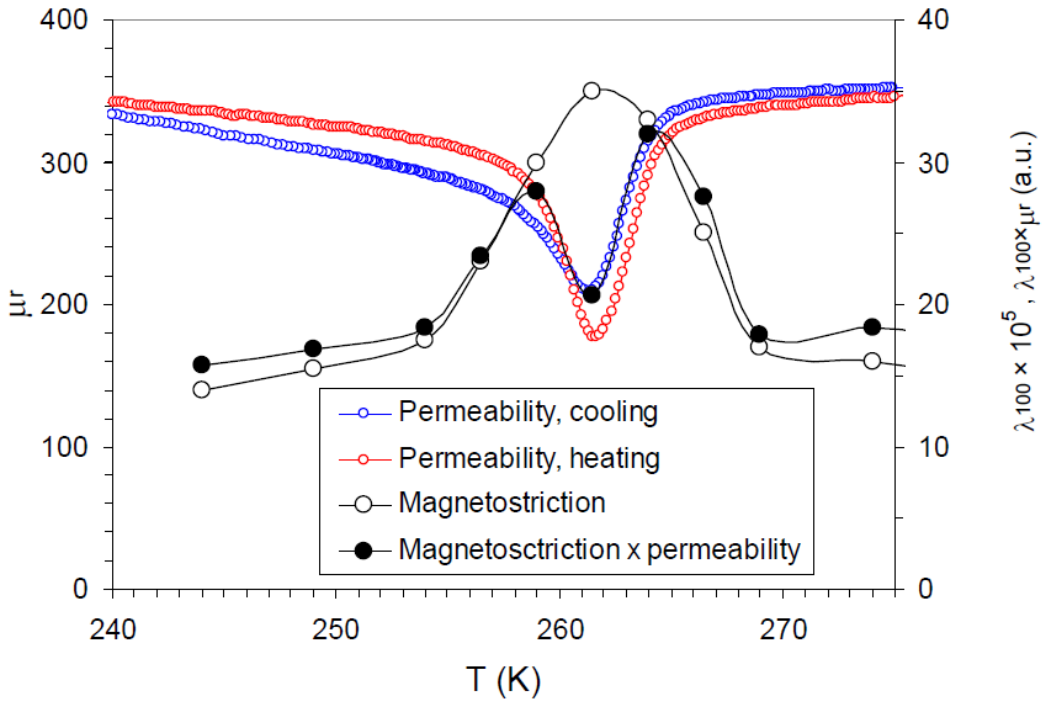

Figure 4.3: Temperature spectra of reversible permeability, μ_r, saturation magnetostriction, λ_{100} (values of taken from 1b of Ref [6]) and of their product $\lambda_{100}x\mu_r$ which is proportional to the microeddy relaxation strength, Δ_μ.

On the other hand, the Macroeddy current relaxation strength is controlled by λ_s (through $(\partial B/\partial\sigma)_H$) and μ_r, as shown in eq. 4.4. In contrast to Δ_μ, the drop of the permeability promotes Macroeddy relaxation. However, the behaviour of $(\partial B/\partial\sigma)_H$ has not been studied in the present work, but it is expected to increase in the same way as saturation magnetostriction, if the possible increase of the saturating field at T_{PM} is less than that of λ_s, which is very likely, since λ_s increases strongly (more than 3 times). Therefore, in contrast to Δ_μ, Δ_M increases notably during the PMT.

4.3. Interpretation of the anelastic and "elastic" phenomena during PMT as due to the eddy current relaxations

Thus, the behaviour during PMT of the two eddy current relaxation frequencies and of the macroeddy relaxation strength accounts for an intense IF peak during PMT. The increase of the macroeddy current relaxation strength makes this peak especially sensitive to applied field, in full agreement with experimental data, Fig. 3.1(a).

The double internal friction peak during PMT is explained by opposite effects of reversible permeability and magnetostriction variations on the microeddy current relaxation strength.

The last point pending interpretation from the list of effects in Section 3.3 is switching between the unusual opposite tendencies in the field dependences of the internal friction and Young´s modulus, observed in the cubic and premartensitic phases, to the tendency typical for a conventional relaxation over the narrow temperature range close to the PMT.

In the cubic and premartensitic phase the field dependence of the total damping and modulus defect follow the pattern shown in Fig. 4.2, when the increase of damping with applied field is concomitant with the increase of the apparent modulus. The analysis performed in Sections 4.2.1 and 4.2.2 indicates that the macroeddy current relaxation is strongly promoted during the PMT both due to the strong increase of the macroeddy relaxation strength and the increase of the macroeddy relaxation frequency. This promotion of the macroeddy current relaxation during the PMT explains the inversion of the effect of the applied field on YM during the PMT (Fig. 3.7(b)) and a strong rise of IF under applied field than that in the cubic phase. Outside the PMT range the Microeddy component of ΔE-effect, which is suppressed by the external magnetic field is predominant over the Macroeddy one at $f \approx 10^5\ Hz$, hiding the characteristic YM decrease due to Macroeddy current relaxation. This competition of Eddy current ΔE-effects results in "anomalous" increase of IF and YM before and after PMT. The higher Macroeddy relaxation strength around PMT promotes the Macroeddy ΔE-effect and thus the normal Macroeddy relaxation behaviour emerges: a YM decrease versus field (for values not reaching the saturating field) is accompanied with an IF increase.

We mention that macroeddy current related effects (both IF and ΔE-effect) require maximum versus applied field, Fig. 4.2. These YM and IF maxima are observed at applied fields close to saturating ones [39, 56] which could not be reached in the present study. The traces of the characteristic for macroeddy current relaxation YM minimum versus field can be seen at higher applied field in the data by Planes et al. [5], see Fig. 1.5.

5. Conclusions:

A new interpretation of a number of elastic and anelastic phenomena during premartensitic transition in Ni2MnGa is proposed based on the concepts of Microeddy and Macroeddy current relaxations, which are associated with respectively with the short-range oscillatory motion of ferromagnetic domain walls and stress-induced variations of the macroscopic magnetization of the sample. The suggested interpretation also explains the contradictory experimental data in previous articles, where the results were obtained by different experimental techniques operating at different frequency ranges.

6. References

[1] G.B. Olson, H. Hartman, Martensite and Life: Displacive Transformations as Biological Processes, *J. Phys. Colloques,* 43, (1982), 855-865.

[2] Salas, D*., Athermal and Isothermal Characteristics in Diffusionless Martensitic Transformations*, UIB (2014).

[3] L. Declaey, P. Haasen (Ed.), Materials Science and Technology, Vol. 5: Phase Transformations in Materials, VCH, Weinheim, (1991), 339.

[4] K. Ullakko et al., Large Magnetic-Field-Induced Strains in Ni2MnGa Single Crystals, *Appl. Phys. Lett.,* 69, (1996), 1966.

[5] Planes, A.; Obradó, E.; Gonzalez-Comas, A.; Mañosa, L.; Premartensitic Transition Driven by Magnetoelastic Interaction in bcc Ferromagnetic Ni2MnGa, *Phys. Rev. Lett.,* 79*,* (1997), 20.

[6] Gonzalez-Comas, A.; Obradó, E.; Mañosa, L.; Planes, A.; Chernenko, V. A.; Hattnik, B. J.; Labarta, A. Premartensitic and martensitic phase transitions in ferromagnetic Ni2MnGa, *The American Physical Society,* 60, (1999), 10.

[7] A. Planes, L. Mañosa, Vibrational Properties of Shape Memory Alloys, *Solid State Phys.,* 55, (2001), 159-267.

[8] X. Ren, K. Taniwaki, K. Otsuka, T. Suzuki, K. Tanaka, Y. I. Chumlyakov, I. Yu, T. Veki, Influence on Zn Addition on Microstructures and Martensitic Transformation in CuZr-based Alloys, *Phylos. Mag. A,* 79, (1999), 31-41.

[9] Seiner H, Heckzo O, Sedlák P, Bodnárová L, Novotný M, Kopecek J, Landa M, Combined effect of structural softening and magneto-elastic coupling on elastic coefficients of Ni-Mn-Ga austenite*, Journal of Alloys and Compounds,* 577S, (2013) S131-S135.

[10] Planes A, Obradó E, Gonzalez-Comas A, Mañosa L, Premartensitic Transition Driven by Magnetoelastic Interaction in bcc Ferromagnetic Ni_2MnGa, *Physical Review Letters*, 79, (1997), 20.

[11] Murray, S. J.; Marioni M. A.; Kukla A. M.; Robinson, J.; O'Handley, R. C.; Allen, S. M., Large Field Induced Strain in Single Crystalline Ni-Mn-Ga Shape Memory Alloy, *J. Appl. Phys.,* 87, (2000), 5774.

[12] Chernenko, V. A.; Cesari, E.; Kokorin, V. V.; Vitenko, N. I., The Development of New Ferromagnetic Shape Memory Alloys in Ni-Mn-Ga Systems, *Scripta Metall Mater,* 33, (1995), 1239-1244.

[13] Gonzalez-Comas, A.; Obradó, E.; Mañosa, Ll.; Planes, A.; Labarta, A. Magnetoelasticity in the Heusler Ni2MnGa Alloy. *Journal of Magnetism and Magnetic Materials***,** 196-197, (1999), 637-638.

[14] Hu, Q.; Li, C.; Yang, R.; Kulkova, S.E.; Bazhanov, D.I.; Johansson, B.; Vitos, L., Site Occupancy, Magnetic Moments and Elastic Constants of Off-Stoichiometric Ni2MnGa from First-Principles Calculations, *Phys. Rev. B* 79, (2009), 144112.

[15] Albertini, F.; Paoluzi, A.; Pareti, L.; Solzi, M.; Righi, L.; Villa, E.; Besseghini, S.; Passaretti, F., Phase Transitions and Magnetic Entropy Change in Mn-rich Ni2MnGa Alloys, *J. App. Phys.*, 100, (2006), 023908.

[16] Ranjan, R.; Banik, S.; Barman, S. R.; Kumar, U.; Mukhopadhyay, P. K.; Pandey, D., Power X-ray Diffraction Study of the Thermoelastic Martensitic Transition in Ni2Mn1.05Ga0.95, *Phys. Rev. B*, 74, (2006), 224443.

[17] L. Mañosa, A. González-Comas, E. Obradó, A. Planes, Anomalies related to the TA2 phonon-mode condensation in the Heusler Ni2MnGa alloy, *Phys. Rev. B, 55,* (1997) 11068-11071.

[18] A. Zheludev, S. M. Shapiro, P. Wochner, A. Schwartz, M. Wall and L. E. Tanner, Phonon Anomaly, Central Peak and Microstructures in Ni2MnGa, *Phys. Rev. B*, 51, (1995) 11319.

[19] V. A. Chernenko, J. Pons, C. Seguí, E. Cesari, Premartensitic Phenomena and other Phase Transformations in Ni-Mn-Ga Studied by Dynamical Mechanical Analysis and Electron Diffraction and *Acta Mater.,* 50, (2002), 53-60.

[20] V. A. Chernenko and V. V. Kokorin, in Proceedings of the International Conference on Martensitic Transformations, edited by C. M. Wayman and J. Perkins, Monterey Inst of Advanced Studies, (1993), p. 1205.

[21] A. N. Vasil'ev, V. V. Kokorin, Y. I. Savchenko, and V. A. Chernenko, The Magnetoelastic Properties of Ni2MnGa Single Crystal, Sov. Phys. JETP 71, (1990), 803.

[22] O. Sodererg, I. Aaltio, Y. Ge, O. Heckzo, S. P. Hannula,Ni-Mn-Ga Multifunctional Compounds, *Matter. Sci. Eng. A*, 481-482, (2008), 80-85.

[23] A. Ayuela, J. Enkovaara, R. M. Nieminen, Ab Initio Study of Tetragonal Variants in Ni2MnGa Alloy, *J. Phys. Condens. Matter.,* 14, (2002) 5325-5336.

[24] Kuznetsov P. V, Vlasov I. V, Skylarova E. A, Smekalina T. V, Formation and evolution of tweed structures on high purity aluminium polycrystalline foils under cyclic tension, *Institute of Strengths Physics and Materials Science,* 1683, (2015), 020118.

[25] Z. H. Nie, Y. Ren, Y. D. Wang, D. M. Liu, D. E. Brown, G.Wang, and L. Zuo, Strain-Induced Dimensionality Crossover and Associated Pseudoelasticity in the Premartensitic Phase of Ni2MnGa, *Appl. Phys. Lett.* 97, (2010), 171905.

[26] S. Singh, J. Nayak, A. Rai, P. Rajput, A. H. Hill, S. R. Barman,and D. Pandey, (3 + 1)D Superspace Description of the Incommensurate Modulation in the Premartensite Phase of Ni2MnGa: A High Resolution Synchrotron X-Ray Powder Diffraction Study, *J. Phys.: Condens. Matter,* 25, (2013), 212203.

[27] H. Seiner, V. Kopecký, M. Landa, O. Heckzo, Elasticity and Magnetism of Ni2MnGa Premartensitic Tweed, *Phys. Status Solidi B,* 251, Issue 10, (2014), 2097-2103.

[28] Worgull, J.; Petti, E.; Trivisonno, J.; Behaviour of the elastic properties near an intermediate phase transition in Ni_2MnGa, *Phys. Rev. B,* 54, (1994), 22.

[29] M. Stipcich, L. Mañosa, A. Planes, Elastic constants of Ni-Mn-Ga magnetic shape-memory alloys. *Phys. Rev. B* 70 (2004), 054115-1.

[30] Salazar Mejía, C, Born, N.; Schiemer, A.; Felzer, C.; Carpenter, M. A.; Nicklas, M. Strain and order parameters in Ni-Mn-Ga Heusler alloys from resonant ultrasound spectroscopy. *Phys. Rev. B.*, 97, (2018), 094410.

[31] Pérez-Landazábal, J. I.; Sánchez-Alarcos, V.; Gómez-Polo, C., Recarte, V.; Chernenko, V. A.; Vibrational and magnetic behaviour of transforming and non-transforming Ni-Mn-Ga alloys. *Phys. Rev. B,* 76, (2007), 092101.

[32] O. Heckzo, H. Seiner, P. Sedlák, J. Kopecek and M. Landa, Anomalous lattice softening of Ni2MnGa austenite due to magnetoelastic coupling, *J. App. Phys.* 111 (2012), 07A929.

[33] K. Ullakko, J. K. Huang, C. Kantner, R. C. O'Handley, V. V. Kokorin, Large Magnetic-Field-Induced Strains in Ni2MnGa Single Crystals, *App. Phys. Lett.* 69 (1996), 1966-1968.

[34] O. Heckzo, A. Sozinov, K. Ullakko, Giant-Field-Induced reversible strain in Magnetic Shape Memory NiMnGa Alloy, *IEEE Trans Magn.* 36, (2000), 3266-3268.

[35] P. Zhao, L. Dai, J. Cullen, M. Wuttig, Magnetic and Elastic Properties of Ni49.0Mn23.5Ga27.5, *Metall Mater. Trans. A 38* (2007), 745-751.

[36] Livingston, J. D. Magnetomechanical Properties of Amorphous Metals, Phys. Stat. Sol. (a) 70, (1982), 591-596.

[37] Kustov, S.; Corró, M.; Kaminskii, V.; Saren, A.; Sozinov, A.; Ullakko, K. Elastic and anelastic phenomena related to eddy currents in cubic Ni2MnGa*, Scr. Mater.***,** 147, (2017), 69-73.

[38] Gaganidze E, Esquinazi P, Vibrating ferromagnet in a magnetic field, *The American Physical Society* 56, (1997), 7823.

[49] Berry, B.S.; Pritchet, W.C. ΔE-effect and Macroeddy-Current Damping in Nickel. *J. Appl. Phys.*, 49, (1978), 1983–1985.

[40] San Juan, J. Mechanical Spectroscopy, *Mater. Sci. Forum.*, 366-368, (2001), 32-73.

[41] Nowick A. S., Berry B. S, Anelastic Relaxation in Crystalline Solids*, Academic Press* (1972).

[42] Degauque, J., Magnetic Domains, *Mater. Sci. Forum.*, 366-368, (2001), 453-482.

[43] W. P. Mason, Domain Wall Relaxation in Nickel, *Phys. Rev.* 83 (1951) 683-684.

[44] W. P. Mason, Rotational Relaxation in Nickel at High Frequencies, *Rev. Mod. Phys.* 25 (1953) 136-139.

[45] C. Zener, Internal Friction in Solids V. General Theory of Macroscopic Eddy Currents, *Phys. Rev.* 53 (1938) 1010-1013.

[46] Smith, G.W.; Birchak, J.R.; Effect of Internal Stress Distribution on Magnetomechanical Damping, *J. Appl. Phys.* 39 (1968) 2311-2316.

[47] Kustov, S. J.; Torrens-Serra, J.; Salje, E. K. H.; Beshers, D. N. Re-entrant Spin Glass Transitions: New Insights from Acoustic Absorption by Domain Walls., *Sci. Rep*. 7, (2017), 16846.

[48] Kustov, S; Golyandin, S.; Ichino, A.; Gremaud, G.; A new design of automated piezoelectric composite oscillator technique. *Mater. Sci. Eng. A***,** 442, (2006), 532-537.

[49] Gremaud. G.; Kustov S.; Bremnes, Ø. Ultrasonic Techniques: PUCOT and ACT, *Mater. Sci. Eng. Forum* **2001,** 366-368, 652-666.

[50] W. H. Robinson, A. Edgar, IEEE Trans. Sonics Ultrasonics SU-21 (1974) 98-105.

[51] Balamuth, L. A new method for measuring elastic moduli and the variation with temperature of the principal Young's modulus of rocksalt beween 78◦K and 273◦K, *Phys. Rev.***,** 45, (1934), 715-720.

[52] Read, T. A. The internal friction of single metal crystals. *Phys. Rev.,* 58, (1940), 371-380.

[53] Wolfenden, A.; Harmouche, M. R.; Hartman Jr., J. T. *J. Phys.* **1985,** 46, C-10-391-C-10-394.

[54] Kosugi, T.; McKay, D.; Granato, A. V.;Theory of Dislocation Tunneling Through a Pinning Point, *J. Alloy Compd.,* 310, (2000), 111-114.

[55] Osborn, J.A. Demagnetizing Factors of the General Ellipsoid. *Phys. Rev.*, 67, (1945), 351-357.

[56] Seiner H, Sedlák P, Bodnárová L, Drahokoupil, J, Kopecký, V, Kopecek J, Landa M, Heckzo, O.; The effect of antiphase boundaries on the elastic properties of Ni-Mn-Ga austenite and premartensite. *J. Phys. Condens. Matter*, 25, (2013), 425402.

[57] Dakon, T.; Hayashi, Y.; Li, D.; Honda, F.; Oomi, G.; Narumi, Y.; Hagiwara, M.; Kanomata, T.; Eto, T. Forced magnetostrictions and magnetizations of $Ni_{2+x}MnGa_{1-x}$ at its Curie temperature, *Materials*, 11, (2018), 2115.

[58] Torrens-Serra, J.; Solivelles, F.; Corró, M.L.; Stoica, M.; Kustov, S.; effect of temperature and magnetic field on magnetomechanical damping of Fe-based bulk metallic glasses, *J. Phys. D. Appl. Phys.,* 49, (2016), 505003.